Synthesis, Characterisation and Evaluation of Biological activity of *Euglena gracilis* derived Nanophytosomes in Ovarian cancer

Synopsis of the thesis to be submitted for the award of the degree of
Doctor of Philosophy in

Faculty of Inter-Disciplinary Research
(BIOCHEMISTRY)

Submitted to

SRI BALAJI VIDYAPEETH

Submitted by

Ms. Varsha V
UIN: 1805003001

Under the guidance of

Dr. Veni Subramanyam
Assistant Professor,
Mahatma Gandhi Medical Advanced Research Institute (MGMARI),
Sri Balaji Vidyapeeth,
Puducherry 607-402, India.

TABLE OF CONTENTS

1. INTRODUCTION 3

2. AIMS AND OBJECTIVES 3

3. HYPOTHESIS 4

4. REVIEW OF LITERATURE 4

4.1 Ovarian cancer 4

4.2 Nanophytosomes - Drug delivery system 4

4.3 *Euglena gracilis* for nanophytosome preparation 5

4.4 Ovarian cancer pathogenesis 5

4.5 Epigenetic modifications 7

5. MATERIALS AND METHODS 8

5.1 Materials required 8

5.2 Cell lines and culture conditions 9

5.3 Synthesis of nanophytosomes 9

5.4 Characterisation of nanophytosomes 9

5.5 *In silico* analysis by Molecular docking and simulation 10

5.6 Cell viability assay 10

5.7 Live/dead staining by AO/EB assay 10

5.8 Cytoplasmic/ nuclear staining by FITC/DAPI 10

5.9 Wound healing assay 11

5.10 Oxidative stress by DCFH-DA 11

5.11 Cell cycle distribution by flow cytometry 11

5.12 3D Spheroids culture and treatment 11

5.13 Quantitative Real-Time PCR 12

5.14 Immunofluorescence study 12

5.15 Enzyme linked Immuno Sorbent Assay (ELISA) 13

5.16 Statistical Analysis 13

6. RESULTS AND DISCUSSION 13

7. SUMMARY AND CONCLUSION 30

8. ABSTRACT 31

9. REFERENCES 31

10. PUBLICATIONS 35

11. PODIUM&POSTER PRESENTATIONS 35

1. INTRODUCTION

Ovarian cancer, the most common gynaecological malignancy, has a poor prognosis and early diagnosis, which demands the development of biomarker discovery. Despite the availability of therapeutic options and medications, ovarian cancer patients continue to face treatment resistance, relapses and poor survival rate. There is a vital need to discover new treatment strategies to address drug resistance and toxicity issues. Medicinal herbs and their phytochemicals are emerging as an excellent therapeutic option for a variety of ailments. However, the low bioavailability and selectivity to the target site limits their clinical utility. Several methods for developing effective carrier systems have been proposed, among which nanoformulations are gaining interest in drug delivery by improving the bioavailability of drugs. Among different nanoformulations, nanophytosomes (NP) are lipid-based carrier drug delivery systems that act as a barrier in protecting the drug from losing its native potential or degradation of the active principles by the physiological secretory enzymes in the living system. The targeted approach towards enhancing the ability of the drug is greatly appreciable with its bioavailability and improved pharmacological and pharmacokinetics of the herbal extracts. In our current study, *Euglena gracilis* (EG), a unicellular alga with multiple health benefits, was developed into NP. The major component of EG is β- 1,3 glucan (BG), possessing several apoptotic and inflammatory activities. BG possesses a heavy molecular weight and triple helical structure with a complex nature. To delineate the BG structure, and to improve its bioavailability, BG was developed into NP. Hence, to understand the effect of the developed NPs in ovarian cancer pathogenesis in an *in vitro* and *in vivo* mimicking model study focussed on apoptosis (Capase3, Caspase8, BAD and BCL-2), cell proliferation (PI3K/AKT/mToR), inflammatory (NFκB), oxidative stress (NRF-2), Migration and Metastasis (MMP-3, MMP-9), JAK/STAT3 pathway (IL-6), Epithelial to mesenchymal transition (EMT) markers (E-cadherin and Vimentin), Cancer stemness (β-catenin), cell cycle regulator (E2F-1) with influence on epigenetic modulators (PRMTs and SIRTs) by gene and protein expression analysis. The effectiveness of NPs and their drug delivery and mechanism of action towards OC pathogenesis was explored and expedited in the review of the literature.

2. AIM AND OBJECTIVES

Aim: To synthesize, characterize, and evaluate the biological effects of β- 1,3 glucan and *Euglena gracilis* derived nanophytosomes in human ovarian cancer.

Objectives of the study

Objective I: To synthesize, standardize, and characterize the nanophytosomes from *Euglena gracilis*

Objective II: To study the effects of nanophytosomes in ovarian cancer cells

Objective III: To investigate the role of nanophytosomes on apoptotic, inflammatory, oxidative stress, and epigenetic markers in ovarian cancer cells by Real-time PCR.

Objective IV: To analyze the downstream protein expression of nanophytosomes in ovarian cancer cells by Immunofluorescence and ELISA.

3. HYPOTHESIS

We hypothesized that the nanophytosomes derived from β- 1,3 glucan and *Euglena gracilis* effectively inhibit ovarian cancer by regulating apoptotic, inflammatory, oxidative stress, and epigenetic pathways.

4. BRIEF REVIEW OF LITERATURE

4.1 Ovarian cancer

Ovarian cancer (OC) is the third most lethal gynaecological malignancy among women contributing to about 2.1% of all cancer deaths with a 5-year survival rate of 49.7% (1) . Based on the statistics of the National Cancer Registry Programme in India, the cumulative risk of OC in India is 1 in 133 with 43,886 patients as of 2020 which contributes to about 3.44% of all cancer cases (2). The risk of OC in India is increasing in the coming years, with current treatment strategies including chemotherapy, immunotherapy, and surgery in later stages, with poor screening. Despite various treatment strategies, the off-target mechanisms and limited response therapy show severe side effects and lower survival rates. The existing targeted therapies for OC target cancer cells and also affect normal cells. Conventional therapies were associated with side effects and minimal survival. Recent evidence suggests that natural compounds, i.e. phytocompounds, were used as adjuvants of traditional chemotherapy in OC. Bioavailability is proportional to drug efficacy which seeks enhancement of absorption to improve efficiency mostly in drug resistance conditions (3). Nanoformulations are the emerging fields in the drug delivery system which has the potential to overcome the limitations of chemotherapeutic drugs. Among these, nanophytosomes a lipid-based drug delivery mechanism which has several advantages, such as improved bioavailability, biocompatibility, and biodegradable properties, thereby improvising therapeutic impact in biological system (4). Thus, nanophytosomes derived from algal natural sources were chosen as an efficient nanocarrier to improve bioavailability in OC.

4.2 Nanophytosomes – Drug delivery system

Nanophytosomes (NPs) are lipid vesicular drug delivery systems that bind the phytoconstituent to phospholipids, and aid in releasing the drug at the target site, enhancing its efficiency with ease of preparation and adaptability (5). In chemotherapeutic systems, NPs show high drug-loading capacity, the ability to dissolve drugs within the inner core, and the ability to selectively accumulate in tumour tissue improving permeability and retention influenced by active or passive targeting (6). For instance, Silybin, a natural flavolignin with hepatoprotective properties, was poorly soluble in water, while silybin phytosome nanosuspension improved its bioavailability and enhanced hepatoprotective efficiency (7). Curcumin phytosome complex was used in pancreatic cancer of Phase-II trial (8). Thus, it has been proposed as a promising candidate for the delivery of insoluble phytochemicals. The NPs of phytocompounds were aesthetic in conservative management, substantially improving conventional therapy by specific targeting and efficient drug delivery. Thus, the NPs were employed from the algal compound *Euglena gracilis* to combat the drug complexities in OC.

4.3 *Euglena gracilis* for Nanophytosome preparation

Euglena (*Euglena gracilis Z*) (EG), a freshwater unicellular photosynthesizing green alga without a cell wall has a store of numerous vitamins and minerals at high concentrations with great industrial, commercial, and biological applications (9). EG comprises 80% of carbohydrate storage material, paramylon which is an insoluble β-1,3 glucan. β-1,3 glucan (BG) is known to have various biological effects on human health which enhances immunological functions involved in treating and preventing infectious oncologic and viral diseases, such as human immunodeficiency virus-HIV, colorectal cancer (10), atopic dermatitis (9), relieving arthritic symptoms in Rheumatoid arthritis condition (11), protective effects on acute-hepatic injury (12), and improved glycemic control in type-II diabetes mellitus (13). Other components include wax esters, composed of C14:0 saturated fatty acid, myristic acid, and myristyl alcohol, synthesized under anaerobic conditions, which helps in the production of biodiesel and jet fuel as an alternative to fossil fuel (14). Aqueous extracts of EG exhibit strong antioxidant, pro-, and anti-inflammatory innate responses and have proven to be effective against lung carcinoma via apoptosis induction in mice (15). EG and BG have not been much explored in ovarian cancer cells. Thus, a novel drug delivery system was employed in the preparation and synthesis of EG and BG-derived NPs. In the present study, the obtained NPs were synthesized, characterized, and studied in the treatment of human OC cells OVCAR-3 and SKOV-3.

4.4 Ovarian cancer Pathogenesis

OC has been known to be called the *"silent killer"* due to its heterogeneous nature, and the symptoms appear late in most of the cases due to poor prognosis as it consists of several histologic characteristics with a complicated pathogenesis process. The pathogenesis of OC begins from dedifferentiation of the underlying ovary, from which several molecular mechanisms arise, which lead to the severity of cancer. In our study, we used human epithelial ovarian adenocarcinoma cell lines OVCAR-3 and SKOV-3 to study the effects of EG and BG-derived NPs. OVCAR-3 was obtained from progressive adenocarcinoma of the ovary, representing the advanced stage, while SKOV-3 was obtained from the ascitic fluid of the ovary, which represents non-serous cystadenocarcinoma. The following are some of the major pathways involved in OC pathogenesis:

4.4.1 Apoptosis (Caspase 3, Caspase 8, BAD, and BCL-2): The pro-apoptotic proteins caspases 3,8 and BAD are majorly involved in the cell death process. Pro-caspase 8 turns to active caspase 8 activating caspase 3 in the initiating phase enters into the intrinsic pathway. Caspase 3 is activated during the execution phase responsible for cell death i.e apoptosis. BCL-2 acts as an antiapoptotic protein inhibits apoptosis and responds to chemotherapy in OC and used as a prognostic indicator in OC progression (16). Apoptosis was reported by several NPs targeting these mechanisms includes leucoselect phytosomes, scorpion-venom functionalized phytosomes loaded with quercetin, thymoquinone phytosomes, andrographolide phytosomes in human lung, breast and liver cancer (17).

4.4.2 Cell proliferation (PI3K/AKT/mTOR): PI3K/AKT/mTOR signalling plays a major role in the carcinogenesis and tumour resistance mechanism of OC. Aberrant activation of this

signalling results in mutation of PIK3CA and AKT, which results in loss of PTEN due to homologous deletions. mTORC1 and mTORC2 have also been found to be involved in the cell migration and proliferation process. Several inhibitors have been developed in clinical and pre-clinical studies to target this pathway for a more therapeutic approach in OC (18). The mTOR inhibitors approved by the FDA and European Medical Association include Temsirolimus and Everolimus for the treatment of OC.

4.4.3 Inflammatory (NFκB): Nuclear factor kappa-light-chain-enhancer of activated B cells (NFκB), transcription factor known to play an important role in activating inflammatory signaling pathways. The interaction between NFκB and estrogen majorly contributes to the pathogenesis of OC. NFκB is regulated by estradiol by degrading inhibitor of nuclear factor κB (IkB) and inhibiting phosphorylation of IkB proteins by IkB kinase (IKK) complex. Hyperactivation of PI3K/AKT/mTOR often results in downstream activation of NFκB which is involved in angiogenesis, proliferation and expression of antiapoptotic genes. Targeted therapeutics with combination therapy of NFκB and anti-estrogen inhibitors have been developed in OC (2). Curcumin phytosomes have shown significant inhibitory effects on NFκB and mTOR activity in contrast to pure curcumin in hepatitis B virus-related hepatocellular carcinoma (19).

4.4.4 Oxidative stress (NRF-2): NRF-2 activation in OC acts by the Keap-1 pathway results in the development of chemoresistance cells, which deactivates drug-mediated oxidative stress and typically results in cell death. NRF-2 levels result in high glutathione (GSH) levels. These high GSH levels have been explained as a response against ROS levels, which acts as a secondary messenger as studied in SKOV-3 and OVCAR-3 cells. NRF-2 levels play a major role in drug resistance by increasing cell antioxidant capacity which is on top priority in developing drugs and inhibitors in response to chemotherapy in OC (20). Luteolin phytosomes inhibited NRF-2 mediated signalling, leading to cell death in breast cancer (21).

4.4.5 Migration and Metastasis (MMP-3, MMP-9): The matrix metalloproteinases (MMPs) are involved in extracellular matrix degradation and found to be upregulated in OC. The activation MMPs results in tumour invasion and metastasis. MMP-3 expression is found in cystic fluids of ovarian tumours and is correlated with activation by MMP-7 and 9. MMP-9 has been involved in the prognosis of OC wherein TGF-β gets activated via its proteolytic conversion. MMP-9 has been highly expressed in advanced malignant tumours of OC. Several inhibitors have been developed to contribute to the therapy of OC (22). Inhibition of MMP-3 by *Zingiber officinale* and *Acmella oleracea* phytosomes was reported in osteoarthritis and silybin phytosome in prostate cancer (23) and curcumin phytosomes inhibited MMP-9 activity in lung cancer (24).

4.4.6 JAK/STAT3 pathway (IL-6): IL-6 secretion facilitates tumour cell growth by suppressing apoptosis and promoting angiogenesis. It is highly involved in the development and progression of OC. Elevated levels of IL-6 are found to be correlated with chemoresistance and poor prognosis. Its invasion route in metastasis process has been linked with Epithelial mesenchymal transition (EMT) and several post-translational proteins. It has

been known to activate MMP-2 and 9 during the invasion process. Several studies reported that IL-6 could act as a prominent biomarker in OC indicating the survival of patients (25). *Boswellia serrata* extract phytosome significantly decreased the serum levels of the pro-inflammatory cytokines IL-6 and TNF-α in acute systemic inflammation.

4.4.7 Epithelial to mesenchymal transition (EMT) markers (E-cadherin and Vimentin): The two key markers of epithelial-mesenchymal transition (EMT) are E-cadherin and vimentin, which represent markers of epithelial and mesenchymal cells, respectively for tumour metastasis. E-cadherin is downregulated in OC and acts as a tumour suppressor. Vimentin is a filamentous protein involved in cell adhesion and migration process. Downregulation of Vimentin was found to increase drug resistance in OC. Vimentin expression differs at different stages of OC which elucidates their different mechanism of action (26). Curcumin phytosomes decreased the levels of E-cadherin and reduced expression of Wnt pathways in colorectal cancer (27).

4.4.8 Cancer stemness (β-catenin): β-catenin is one of the key mediators of Wnt pathway. β-catenin has been known to regulate cell proliferation, and apoptosis is majorly involved in the initiation and progression of OC cells. They also play major role in chemoresistance and cell survival, thereby could act as a therapeutic target in OC. Hyperactivation of β-catenin has been seen in advanced grade OC, and thus, inhibition of this pathway can open new avenues in the therapy of OC (28).

4.4.9 Cell cycle regulator (E2F-1): E2F-1 belong to a family of transcription factors majorly involved in cell cycle progression, DNA repair, DNA replication and apoptosis. It is highly expressed and acts as a prognostic indicator in OC. As a cell cycle regulator, its complex disruption makes E2F1 prepared for progression into the late G1/S phase (29). Phytosome loaded with biosynthesized Ag NPs combated bone cancer by targeting E2F-1 factor (30).

4.5 Epigenetic modifications

Epigenetic regulators play a critical role in regulating gene expression without modifying DNA sequences, and are also involved in ovarian cancer tumorigenesis. Among several epigenetic markers, Protein Arginine methyltransferases (PRMTs) and Sirtuins (SIRTs), belonging to the group of Histone deacetylases (HDACs), are prominent epigenetic regulators associated with diverse biological processes, including DNA damage response, apoptosis, protein degradation, and metabolism (31).PRMTs are one of the profound arginine methyltransferases involved in post-translational methylation of different types of cancer, while SIRTs belong to the class III histone deacetylase family of enzymes, nicotinamide adenine dinucleotide (NAD)+-dependent deacetylases, which are known to play diverse roles in regulating metabolic disorders, cell proliferation, and are implicated in mammalian ageing, including cancers and neurodegenerative diseases. PRMTs are classified into four types, with types I and II being the most common types. Type I included PRMT1, 2, 3, 4, 6, and 8 with asymmetric dimethylation. Type II includes PRMT 5 and 9 with symmetric demethylation (32), while SIRTs are classified into four classes: Class I (SIRT 1,2,3), Class II (SIRT 4), Class III (SIRT 5), and Class IV (SIRT6,7) (33). The role of different isoforms of PRMTs and

SIRTs in OC targeted by several mechanisms has been shown in Figure 1. Several HDAC inhibitors have been developed to treat OC which are currently in clinical trials. The role of NPs in the epigenetic mechanisms has been unexplored. However, the NPs target other mechanisms such as oxidative stress and inflammatory processes that majorly contribute to the epigenetic process, such as DNA methylation, Histone acetylation, and deacetylation process. Thus, the role of NPs was employed in understanding the mechanisms of PRMTs and SIRTs to explore therapeutic applications in the treatment of OC.

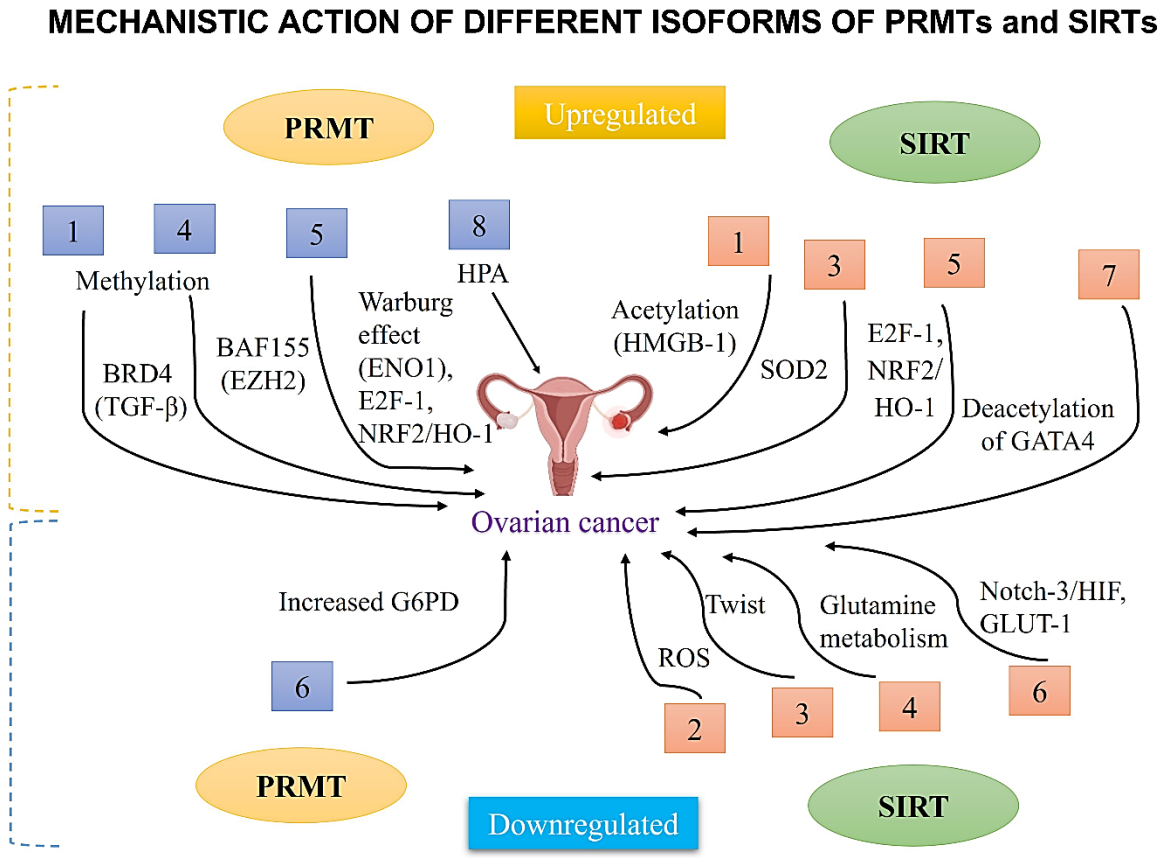

Figure 1. Represents the action of different isoforms of PRMTs and SIRTs by their regulation mechanism in ovarian cancer. Abbreviations: BRD4 – Bromodomain containing 4; TGF-β - Transforming growth factor-beta; BAF155 – BRG (Brahma-related gene 1)/BRM (Brahma) associated factor 155; ENO1 – Enolase 1; E2F-1 - E2F transcription factor 1; NRF2/OH-1 - Nuclear factor erythroid 2-related factor 2/ heme oxygenase-1; HPA – Human Protein Atlas; HMGB-1 – High Mobility Group Box-1; SOD – Super Oxide Dismutase; GATA4- Transcription factor for Cardiac development; HIF- Hypoxia-inducible factor; GLUT-1 - Glucose transporter 1; ROS – Reactive Oxygen Species; G6PD - glucose-6-phosphate dehydrogenase

5. MATERIALS AND METHODS

5.1 Materials required

Euglena gracilis powder extract was purchased from CN Lab Nutrition, Asian group, China. β-1,3-glucan (Paramylon) and Phosphatidylcholine (PC) from Sigma Aldrich, USA. The solvents Dimethylsulfoxide, Ethanol, Methanol and Chloroform were of analytical grade from Sigma

Aldrich,USA. The antibodies NRF-2, NFκB p50, E-cadherin, β-catenin and Vimentin used in this study were from Santa Cruz Biotechnology, USA.

5.2 Cell lines and culture conditions

The human ovarian adenocarcinoma cell lines OVCAR-3, SKOV-3 and human embryonic kidney cells transfected HEK293T were used in this study. OVCAR-3 was a kind gift from Dr. Ramray Bhat, Professor, Indian Institute of Science (IISc), Bangalore, India. SKOV-3 and HEK293T were procured from National Center for Cell Science (NCCS), Pune, India. OVCAR-3 and SKOV-3 cells were cultured in RPMI 1640 and McCoy's 5A media with 10% FBS (Gibco) and 1% Pen/strep (Gibco) antibiotics. HEK293T was cultured in DMEM medium with 10% FBS. For propagation of cells, the cell lines were maintained at 37°C, 5% CO_2 in the incubator. The medium was changed every 2 days once.

5.3 Synthesis of Nanophytosomes

5.3.1 Synthesis of β- 1,3 glucan nanophytosome (BGPC)

60mg of PC was dissolved in chloroform and 40 mg of BG was dissolved in DMSO. BG was heated at 60°C in a water bath for 3h to delineate its triple helical synthesis prior to synthesis. PC and BG were then added dropwise under continuous magnetic stirring for overnight synthesis. The prepared mixture was then processed in a solvent rotary evaporator at 60°C for 3h. Due to the presence of DMSO, the mixture did not evaporate completely. Thus, the remaining mixture was processed in a lyophilizer. Lyophilisation was carried out by keeping the BGPC mixture at -80°C for 4h. The mixture was lyophilized and a thin film of BGPC NPs was obtained. The obtained final mixture was refluxed with nitrogen to remove any traces of solvent in the mixture and stored at 4°C for future use.

5.3.2 Synthesis of Euglena gracilis nanophytosome (EGPC)

Euglena extract powder was added to methanol and centrifuged at 11000 rpm for 30 minutes. The obtained supernatant was again centrifuged at 11000 rpm for 30 minutes. The supernatant obtained was then taken for synthesis of *EG* NPs. 100mg of PC in chloroform and 100mg of EG extract supernatant were added in a ratio of 1:1 dropwise under continuous stirring for overnight synthesis. The mixture was then kept rotary evaporator at 60°C for 1h. The solvents evaporated and a thin film of EGPC was obtained. The obtained mixture was scraped off and refluxed with nitrogen and stored at 4°C for future use (34).

5.4 Characterisation of nanophytosomes

By using the solvent evaporation technique, we were able to standardize the size and stability of BG and EG NPs. We then verified these results using various techniques such as dynamic light scattering (DLS) to determine the size of NPs, zeta potential for NP stability, Fourier transform infrared (FTIR) for chemical group characterisation, X-ray diffraction (XRD) for structural nature, scanning electron microscopy (SEM) for surface modification, high-resolution transmission electron microscopy (HRTEM) for internal structure encapsulation, and entrapment efficiency by UV-visible spectrophotometer and HR-LCMS/MS.

5.5 *In silico* analysis by Molecular docking and simulation

The protein structures of human Protein Arginine Methyltransferase (PRMT 1,3,4,5,6,8) and sirtuins (SIRT1,2,3,5,6) were retrieved from the RCSB Protein Data Bank (PDB) (https://www.rcsb.org/). The structure of BG was generated in the Ligand Builder module of Schrödinger. Ligands were prepared using the LigPrep module of Schrödinger. Docking analysis against PRMTs and SIRTs was performed using the Glide module of Schrodinger using a standard precision algorithm (35). The docked poses were further refined by Molecular Mechanics- Generalized Born Surface Area (MMGBSA) using VGSB solvation model. Molecular Dynamics (MD) simulation for 150 ns was performed using the DESMOND module by Schrödinger (Schrödinger release 2021). OPLS4 force field was utilized. The simulation was performed using the NPT assembly class at a temperature of 300 K and atmospheric pressure of 1.013 bar.

5.6 Cell Viability Assay

MTT (3-(4,5-dimethylthiazol-2-yl)-2,5-diphenyltetrazolium bromide) was used to assess the cytotoxic effect of drugs in OVCAR-3 and SKOV-3 cells. The cells at a density of 5×10^3cells/well were seeded in 96 well plates in triplicates. The synchronized cells were treated in serum-free media for 24 and 48h. At the end of treatment, the cells were washed with PBS. 20 µL of MTT (5 mg/mL) (Sigma) was added to each well and cells were incubated for 4h. An organic solvent dimethyl sulfoxide was added to dissolve the formazan crystals. The absorbance was measured at 570nm using a spectrophotometer (MultiskanGO Thermo Scientific, USA). Cell viability was calculated according to the following equation:

Cell viability (%) = $(\text{Absorbance}_{\text{test-blank}} / \text{Absorbance}_{\text{control-blank}}) \times 100$ (36).

5.7 Live/dead staining by AO/EB assay

The OVCAR-3 & SKOV-3 cells were seeded at a density of 5 X 10^4 cells/well in a 24-well plate and were treated with BG, EG, BGPC and EGPC along with control. The cells were incubated for 48h at 37°C. Cells were washed with PBS and 50 µL each of AO and EB stain was added to wells with a stock concentration of 1 mg/mL in deionized water each. The stain was thoroughly added to all parts of the well and removed, followed by PBS wash. The cells were viewed under a Trinocular inverted fluorescence phase-contrast microscope (Zeiss Axiovert 40 CFL) at a magnification of 20X under UV-lamp.

Total number of cells = No. of live cells + No. of dead cells

% of Number of Live/ dead cells = No. of live or dead cells / Total number of cells X 100

5.8 Cytoplasmic/ nuclear staining by FITC/DAPI

DAPI stain stock was prepared with 5mg/mL in deionized water and FITC was prepared with 1mg/mL stock in acetone. From which 100 µg/mL of working standard was prepared for both FITC and DAPI. Treatment conditions were the same as for AO/EB stain. From which, 50µL of each stain was added to each well followed by PBS wash and viewed under a Trinocular inverted fluorescence phase-contrast microscope (Zeiss Axiovert 40 CFL) microscope with a

magnification of 20X under UV-lamp with green and red filters. The individually taken pictures of FITC and DAPI were then merged via ImageJ software

5.9 Wound Healing assay

The OVCAR-3 & SKOV-3 cells were seeded at a density of 5 X 10^4cells/well in a 24-well plate. Upon cells confluency of 80-90% after 24h, a 200 µL sterile tip was used to mark a straight cell-free wound in all the wells followed by PBS wash twice to remove all the peeled cells and cellular debris. The cells were then treated with IC_{50} of 50 µg/mL of BG, EG, BGPC & EGPC along with control for 48h. The cells migrated into the scratched wound were marked and selected fields were photographed under an inverted phase-contrast microscopy.

$$\%\text{Wound closure rate} = \frac{\text{Distance covered by treated cells}}{\text{Distance covered by control cells}} \text{ X } 100$$

5.10 Oxidative stress by DCFH-DA

The ROS detection was analysed by DCFDA fluorescence stain. 2 X 10^4 OVCAR-3 and SKOV-3 cells/well were seeded in a 24-well cell culture plate. Upon 48 h treatment with IC_{50} of NPs, the cells were washed with 1X PBS. 50 µL of DCFDA stain was added to each well and incubated for 10 min. The cells were then visualised under fluorescent microscope.

5.11 Cell cycle analysis by Flow cytometry

For cell cycle analysis, 1×10^6 OVCAR-3 and SKOV-3 cells per well were seeded in 60-mm Petri dishes. Followed by drug treatment with IC_{50} of NPs for 24 h, cells were subjected to trypsinization and washed twice with PBS. Cells were fixed with 0.5 mL 1X PBS and 4.5 mL of 70% cold ethanol was added under vortex to ensure proper fixation and kept overnight at 4°C. The cells were centrifuged at 1500 rpm to remove the ethanol and washed with 1X PBS twice. Following, the cells were treated with 20 µg/mL RNase A, followed by PI staining (10 µg/mL) at 37°C and incubated in the dark for 30 min. The DNA content and cell cycle distribution were analyzed by flow cytometry using a FACS Calibur instrument (BD Biosciences, San Jose, CA, USA).

5.12 3D spheroids culture and treatment

The cell lines OVCAR-3 and SKOV-3 were grown in their standard culture conditions, harvested, and dissociated into single cell suspensions for spheroid generation. Cells were seeded with a density of 5000 cells/well in the ultra-low attachment (ULA) round-bottom 96-well plates (Corning) in a volume of 200 µL/well culture medium as used in 2D cultures. Plates were incubated at 37°C in 5% CO_2 and spheroids were maintained by performing 50% medium replenishments every 3–4 days. The cells seeded were considered day 0, the spheroids take 3 days to reach the diameter ranging from 250-750 µm. Upon reaching the desired size, the treatment was given on day 4, by aspiring the old media 50% with treatment groups control, BG, EG, BGPC and EGPC with different concentrations ranging from 50–150 µg/mL. The treatment was kept for 48h, followed by images captured in a Phase contrast microscope to measure the spheroid size at 10X magnification. To measure changes in spheroid volume, images were taken pre-treatment (day 4), and post-treatment (day 6). Significant differences in

% Size diameter of spheroid between the control and drug-treated spheroids were calculated using repeated measures two-way ANOVA analyses. The % Size diameter of spheroid was calculated by formula:

$$\%\text{Size diameter} = \frac{\text{Size of treated spheroid}}{\text{Size of control spheroid}} \text{ X } 100 \quad (37)$$

5.13 Quantitative Real-time PCR (qPCR)

For qPCR analysis, 1.5 X 10^5 OVCAR-3 and SKOV-3 cells were seeded in 6-well culture plates and allowed to adhere for 24 h. The cells were treated with IC_{50} concentration of treatment groups for 24 and 48 h, proceeded by RNA isolation using the TRIzol reagent. cDNA synthesis (Verso c-DNA Kit, Thermo Fisher Scientific) was performed using reverse-transcriptase in conventional PCR. The reverse transcription program was followed as per the instructions in the manual under the conditions, cDNA synthesis: 42°C; 30 min; 1 cycle, Inactivation: 95°C; 2 min ;1 cycle. The cDNA samples were diluted with 1:10 ratio. Gene expression analysis of following markers was performed in Real-time PCR (BIORAD CFX96 Touch Realtime system, USA) using the reference gene β-actin and fluorescent dye SYBR green master mix (Applied Biosystems) was used for detection. Primers were designed using Primer 3 software. The fold change was calculated by $2^{(-\Delta\Delta CT)}$ based on Livak's method (Livak & Schmittgen, 2001). The conditions maintained during qPCR includes Initial denaturation: 95°C for 30 s; Denaturation: 95°C for 10 s; Annealing (Tm): 56.3°C for 30 s; Extension: 72°C for 15 s with 39 cycles; upon insertion of melt curve step, 65°C for 0.05 s and 95°C for 0.5 s.

Table 1: List of forward and reverse primers for RT-PCR

S.No.	Gene	Forward (5'→ 3')	Reverse (5' →3')	Product (bp)
1.	PIK3CA	TGGTGCCACTGATACGAGTT	ACCCTGCATGACCATCAAGA	169
2.	AKT2	GGCACGAGAGAAAGCTGATG	TCGTCTCAGGTTCCCAGAAC	221
3.	mTORC1	GTAAGTGGTGAGAGGCCCTT	TGAAGGCAGAAGGTCGGAAT	191
4.	Caspase3	ACCTCTGCACTCCCTTTCTC	TAAACCAAGTCCGTCCCTCC	220
5.	Caspase8	CTGGAGGAAGTGGACAGTGT	CTCAAGGCTTCTCTGGGTCA	180
6.	BAD	AGTCACTCACCTTCCACCTG	CCAGCTCTCCCTGTTGTACA	198
7.	BCL-2	TGATGTGAGTCTGGGCTGAG	GAACGCTTTGTCCAGAGGAG	152
8.	IL-6	GAAAGGAGGTGGGTAGGCTT	AGGTGGGCATGGATTTCAGA	240
9.	E2F-1	AGGCGTGAGGTAGGTTTTGA	GCAATGCTACGAAGGTCCTG	177
10.	NRF2	TGAGCCCAGTATCAGCAACA	AGTGAAATGCCGGAGTCAGA	171
11.	MMP-3	CTCACCCACTTGTCACCTCT	TGGATATCAGATGGTCGGCC	160
12.	PRMT4	CCATGACACGCCTCATTCAG	CTCACCACTACAAGGAGGCA	180
13.	PRMT5	ATGGCAGAGTATGAGGGTGTG	TGGACGGATACCTGTGTGGA	193
14.	SIRT1	GCCGGAAACAATACCTCCAC	ACCCCAGCTCCAGTTAGAAC	174
15.	SIRT5	CGTAGCAGGAGTGACAAGGAA	TGCAGTCTATAGCCCACCT	110
16.	β-actin	ACTCTTCCAGCCTTCCTTCC	CGTACAGGTCTTTGCGGATG	199

5.14 Immunofluorescence study

Immunofluorescence staining was performed in OVCAR-3 and SKOV-3 cells seeded in a concentration of 5000 cells/well in 96-well black clear bottom dishes. The cells were treated with IC_{50} concentrations of BG, EG, BGPC & EGPC along with control. After the drug treatment, the formaldehyde fixed cells were permeabilized using 0.5% saponin, blocked with

1% BSA in PBS (Phosphate Buffered Saline) and incubated with primary antibodies. The primary antibodies used were NRF-2 (C-20) rabbit polyclonal IgG; NFκB p50 (E-10), β-catenin, E-cadherin (G-10) mouse monoclonal IgG1, and Vimentin. The antirabbit antibody conjugated with Alexa Fluor-488 was used as secondary antibody. The nucleus was counterstained with 4′, 6-diamidino-2- phenylindole (DAPI) (Sigma-Aldrich). Further the cells were incubated with secondary antibody, goat anti-rabbit (1:500, Invitrogen, A11034) conjugated with Alexa-488 fluorescence dye, for an hour. The image acquisition was done using Operetta high content imaging system (PerkinElmer, Waltham, MA). The experiment was performed in triplicates. Fluorescent intensity of images was measured by Image J software.

Correlated Total Cell Fluorescence (CTCF) = Integrated Density − (Area of selected cells × Average Background Mean)

5.15 Enzyme linked Immuno Sorbent Assay (ELISA)

ELISA was performed for 2D and 3D culture supernatant treated with IC_{50} concentration of NPs in cultures of OVCAR-3 and SKOV-3. The standard curve was obtained by adding diluted standard 50 µL to the standard well. While in case of sample wells, sample diluent 40 µL was added to testing sample well. Then sample 10 µL was added to testing sample well, blank well was kept empty. The plate was covered and incubated for 45 minutes at 37°C. Then each well was aspirated and washed, repeating the process four times for a total of five washes, 1-3 minutes per time. the plate and blotted it against clean paper towels. The HRP-Conjugated detection antibody 50 µL was added to each well, except the blank well. The plate was covered and incubated for 30 minutes at 37°C. The aspiration/wash process was repeated for five times, as mentioned above. The chromogen solution A 50 µL and chromogen solution B 50 µL was added to each well. The plates were then incubated for 15 minutes at 37°C, protected from light. 50 µL stop Solution was added to each well. The colour in the wells changed from blue to yellow. The ELISA plate was then read at the Optical Density (O.D.) at 450 nm using a microtiter plate reader within 15 minutes**.**

5.16 Statistical Analysis

All experiment data were represented as error bars which shows mean ± SD of three replicates of the experiment. The statistical significance was performed using Two-way Analysis of Variance (ANOVA). Values with $p<0.05,0.01,0.001$ were considered significant. All statistical analyses were done by GraphPad Prism software (GraphPad Software, Inc., CA, USA). All image quantification was performed by Image J software.

6. RESULTS AND DISCUSSION

6.1 Standardization and Characterisation of Nanophytosomes

Solvent evaporation technique was used to optimise the development of these NPs, using different temperatures and lengths of time. BGPC with a size of 134.62 nm was shown to have an optimal response to 60°C for 3h, while EGPC had an optimal size at 158.38 nm without heating (Figure 2A). Given the importance of size in the development of novel particles, the size attained by DLS was a crucial starting point for optimisation. The BGPC and EGPC zeta

potential activity increased the stability of the NPs to 8.28 and -30.38 mV, respectively, which determines the charge on NPs (Figure 2B). Comparing the chemical profiles and interactions of BGPC and EGPC to those of PC, BG, and EG revealed clear variations in the peak displaying different intermolecular interactions (Figure 2D). The XRD structural study of the NPs revealed that the crystalline BG changed into the amorphous BGPC and that the NP production was also influenced by notable peak shifts in the EGPC (Figure 2C). In order to synthesise nanomaterials for medication absorption and bioavailability, size and surface chemistry were crucial, and the nano-size range is effective in overcoming permeability barriers. When compared to the non-derived ones, the surface morphology study using SEM showed alterations in the BGPC and EGPC structures (Figure 2E). When creating the matrix, the TEM analysis aids in comprehending the interior environment and drug entrapment in the PC. At a scale of 100 nm, the BGPC and EGPC displayed spherical and distinct vesicles (Figure 2F). The optimal entrapment efficiency for increasing bioavailability was reported for both BGPC and EGPC NPs, with results showing 82 ± 1.62 and 87 ± 3.22 %, respectively (34). To further study the entrapment efficiency by mass of the NPs, HR-LCMS/MS analysis was performed. The chromatogram from Figure 2A represents the peaks obtained for lipid phosphatidylcholine. The acquisition time from 13.5 min shows a peak rise with variation till 17 min. From Figure 3A, the mass spectra graph at 15.644 min, shows an ejection at 184 Da, which represents the release of the choline group, and the peak at 716.517 represents the signature of PC. The size of BG from *Euglena gracilis* was about 500 kDa. The BG used in the current study was in pure form. Figure 3B shows a distinctive sharp peak at 9 min and shows a mass peak of about 568.2918 (Figure 3B), which displays the signature peak of BG. Considering BGPC, the NP form of BG, it shows different peak graphs from 13.4 to 15.937 min, which resembles that of PC. There is a small peak at 9.47 min, which resembles that of BG, and a similar mass of around 520.3364 was observed, which confirms the presence of BG in BGPC (Figure 3D). One of the major components of EG is BG which comprises 50-70% of total weight. Thus, from the peaks obtained, the peak at 8.96 min shows a mass of 568.29 which resembles that of BG, thereby confirming the presence of BG in EG. The other half of EG comprises wax esters and lipids, and thus, a varied number of peaks were obtained from 12- 20.5 min, which represents the different types of lipids present (Figure 3C). Considering EGPC, the nanoformulation of EG, the peaks were obtained from 11.8 to 16 min with the highest peak value at 14.521 min, which resembles that of BGPC. The distortion of peaks at 1 min in EG to a very small peak obtained in EGPC shows the synthesis and incorporation of EG into PC. The BG peak obtained at 8.9 min was very small in EGPC showing the breakdown of BG compound within EGPC. The EGPC mass spectra show a mass of 593.27 same as found in EG, which confirms the presence of BG in both (Figure 3E) (Published in MethodsX, Varsha Virendra Palol et al.,2023).

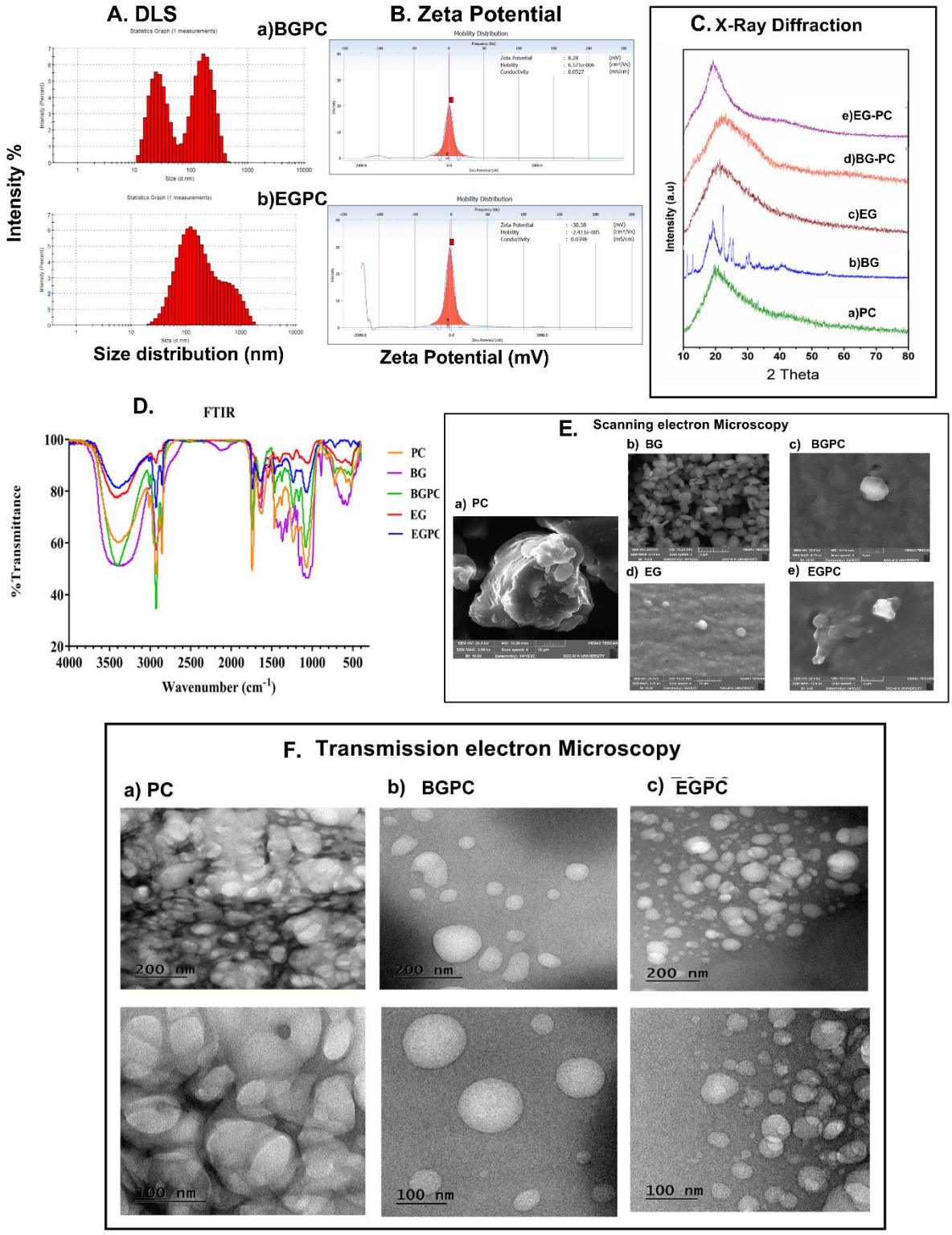

Figure 2 A. Size distribution of NPs by Dynamic Light scattering (DLS), **B.** Stability of NPs by Zeta potential, **C.** Structure determination by X-Ray diffraction, **D.** Chemical group characterisation by Fourier transform infrared (FTIR), **E.** Surface modification by scanning electron microscopy (SEM) at different scales of 2.5 and 10 µm, **F.** Internal structure encapsulation by high-resolution transmission electron microscopy (HRTEM) at various scales of 200 and 100 nm with n = 3.

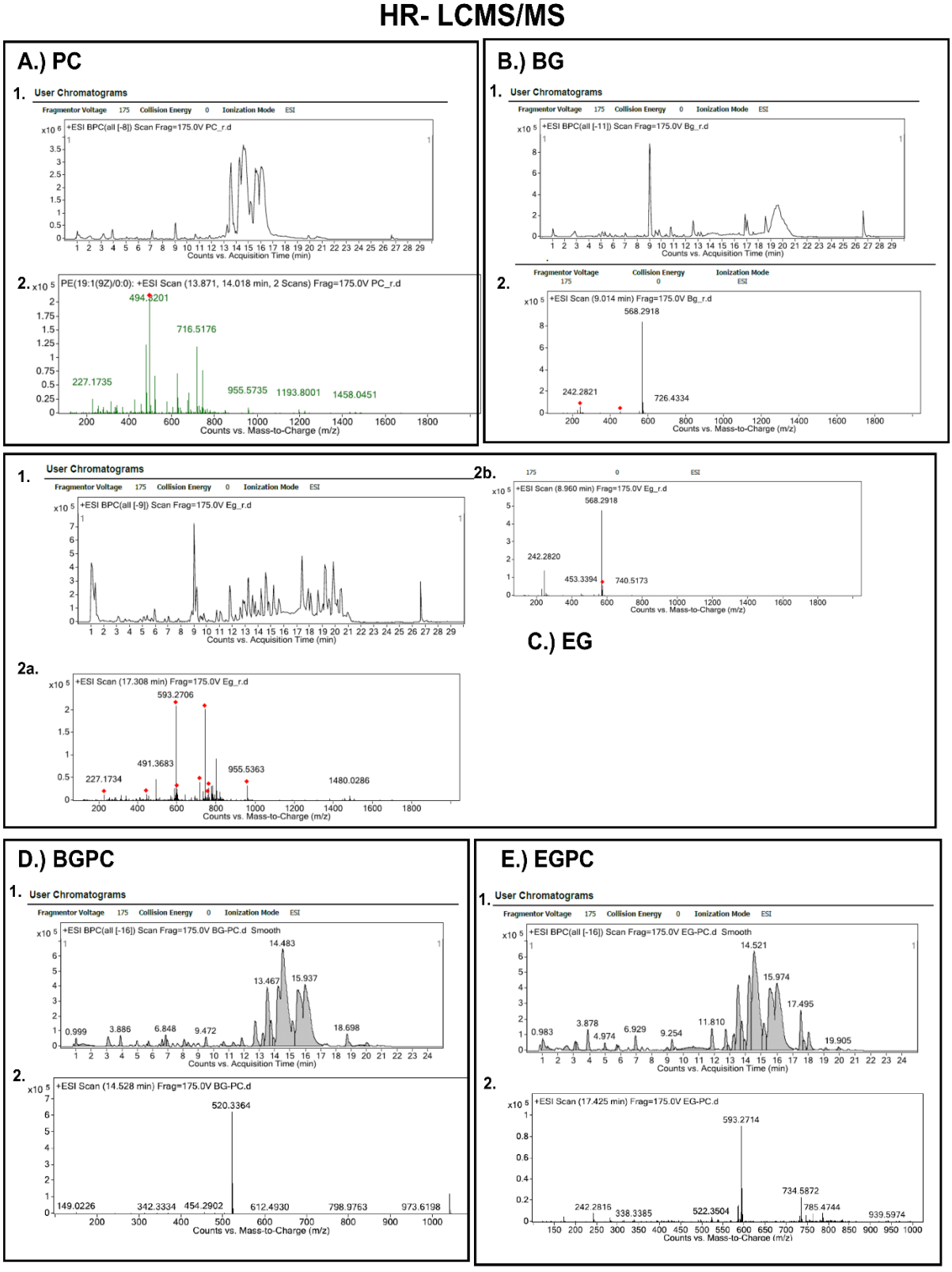

Figure 3. HR-LCMS/MS graphs of A.) PC, B.) BG, C.) EG, D.) BGPC and E.) EGPC to determine entrapment efficiency by mass, where 1. and 2. represents respective MS chromatograms and mass spectra of respective compounds as mentioned.

6.2 *In silico* studies of epigenetic modulators PRMTs and SIRTs by Molecular docking and simulation

6.2.1 Molecular docking

Molecular docking analysis was performed to identify the binding sites of BG on PRMTs and SIRTs. The docking protocol was validated using known co-crystallized ligands of PRMTs and SIRTs. The binding affinities of BG with PRMT and SIRT proteins were assessed using predicted binding energy and binding energy difference ΔG. Further, among the ligand-protein docked complexes, the complex with the lowest ΔG was considered for further simulation analysis.

Among the PRMT variants, PRMT5-BG complex have demonstrated the lowest free binding energy, measuring -65.5 kcal/mol in comparison to their co-crystallized ligand CUX respectively. Thus, for further interactive studies, PRMT5-BG complex was considered. Based on residual analysis of PRMT5, Pro314, Tyr324, Glu328, Gly365, Glu392, Asp419, Met420, Glu435, Glu444, and Cys449 were shown to assist BG with stronger binding affinity. Additionally, the BG forms several H-bond interactions with Gln444, Met420, Asp317, Glu392, Lys393, Glu435, Pro314, and Tyr324 which plays a crucial role in ligand binding specificity (Figure 4A&B). Among the BG-interacting residues of PRMT5, Tyr324, Glu328, Gly365, and Glu444 were found to be essential as similar to the binding of the known co-crystallized ligand CUX. Furthermore, an earlier study highlighted the importance of Glu435 and Glu444 in the catalytic function of PRMT5 (38). Based on these observations, it was reasonable to anticipate that BG binding would inhibit the catalytic function of PRMT5.

In the case of SIRT proteins, SIRT5-BG complex have shown the lowest binding energy of -68.2 kcal/mol in comparison to their co-crystallized ligand MCM respectively. Thus, for further interactive and simulation studies, SIRT5-BG complex was considered. The residual interaction analysis of SIRT5 was facilitated by Arg71, Tyr102, Arg105, Gln140, Val221, and Glu225 which assisted in stronger binding affinity of BG (Figure 4D&E). Of these, Tyr102, Arg105, and Gln140 were found to be involved in the binding of the known co-crystallized ligand MCM, indicating that BG might be a potential inhibitor of SIRT5. Moreover, Arg105 and Tyr102 of SIRT5 form hydrogen and electrostatic interactions with BG and the known ligand MCM to facilitate their binding with SIRT5. Based on these observations, it was anticipated that the binding of BG would inhibit SIRT5 catalytic function.

6.2.2 Molecular simulation

MD simulation of the PRMT5-BG complex revealed that the binding of BG at the active site of PRMT5 does not affect the overall structural integrity of the protein and binds more firmly within the active site. The RMSD value of BG at the active site of PRMT5 was around an average value of 2.42 Å, whereas Cα atoms of the PRMT5 complex were found to fluctuate around an average value of 3.0 Å indicating the stable nature of the complex. RMSD analysis of the Cα atom showed that the binding of BG did not increase by more than 4 Å, signifying the overall stability of the protein throughout the simulation. Similarly, RMSD analysis of BG revealed that the binding of PRMT5-BG complex was more stable within the active site of the ligand RMSD, which also remained within 4 Å throughout the simulation (Figure 5.1A).

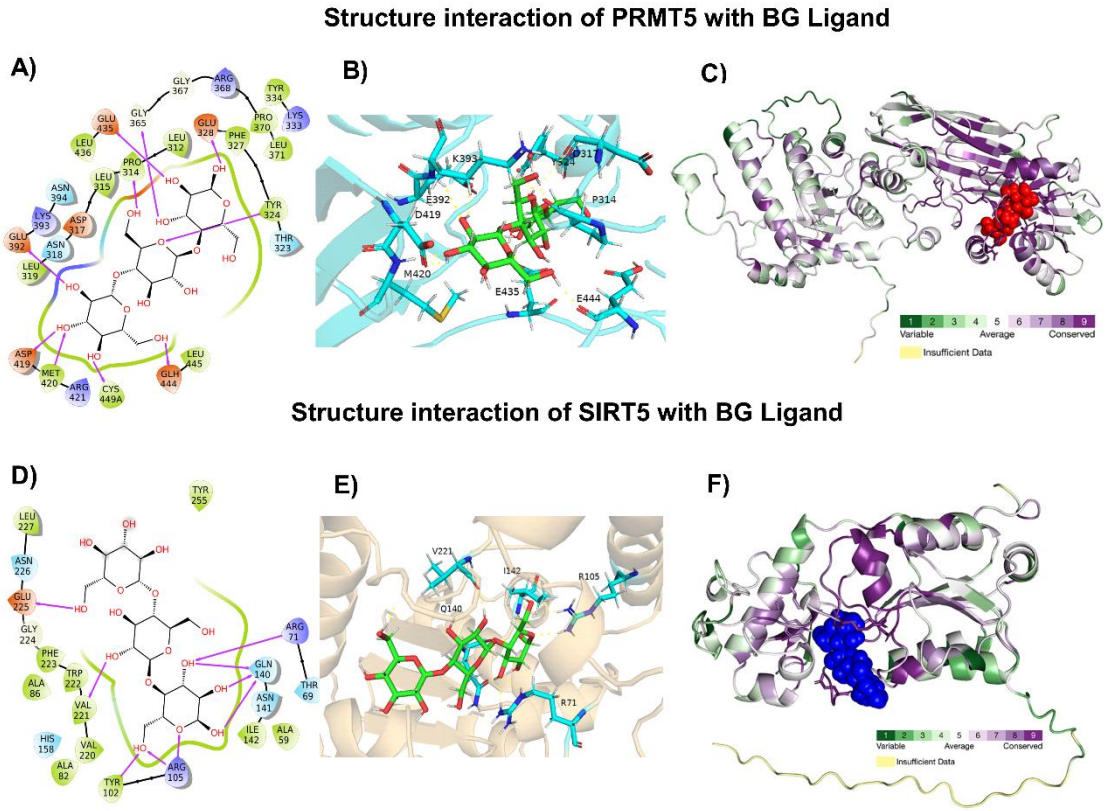

Figure 4. H-bond interactions with the BG ligand in **A)** PRMT5 2D structure, **B)** PRMT5 3D structure, **D)** SIRT5 2D structure, and **E)** SIRT5 3D structure. The H-bonds are represented by violet lines in the 2D structures and yellow lines in the 3D structures. ConSurf analysis of **C)** PRMT5-BG and **F)** SIRT5-BG docked complex to show the residue interaction in different regions. The protein structure is coloured based on the variable and conserved regions, as explained in the legend.

The strength of these hydrogen bond interactions was 91% for Tyr324, 43% for Tyr334, 85% for Glu328, 60% for Asp419, 35% for Met420, and 77% and 56% for Glu392, as it forms two hydrogen bonds with BG at the active site. Interestingly, Glu435, which is reported to be crucial for catalytic activity, forms two hydrogen bonds with strengths of approximately 58% and 71%. The active site, Cys449, was found to interact with one of the water bridges by approximately 32% (Figure 5.1B). The simulation analysis of the SIRT5-BG complex was performed and analyzed on several parameters. To determine the stability of the complex, the RMSD value was calculated. The RMSD value of BG at the SIRT5 active site was found to be around 2.54 Å on average, whereas the Cα atoms of the SIRT5 complex varied approximately by 1.77 Å on average. The BG ligand RMSD and Cα atoms of the SIRT5 complex were determined to be within 4 Å, indicating the stable nature of the SIRT5-BG complex. (Figure 5.2A). Throughout the simulation, at the active site, BG formed more than 10 H-bond interactions, primarily with Tyr102 of approximately 48% and Val221 of approximately 55% strength in SIRT5. Asp143 interacted with BG through water bridge interactions (52% strength) and H-bond interaction (strength 48%. (Figure 5.2B). Within the active site, BG binding was further stabilized by H-bond interactions with Glu225 (40% strength). Other detailed H-bond interactions between the active site residues and BG were shown in Figure 5.2C.

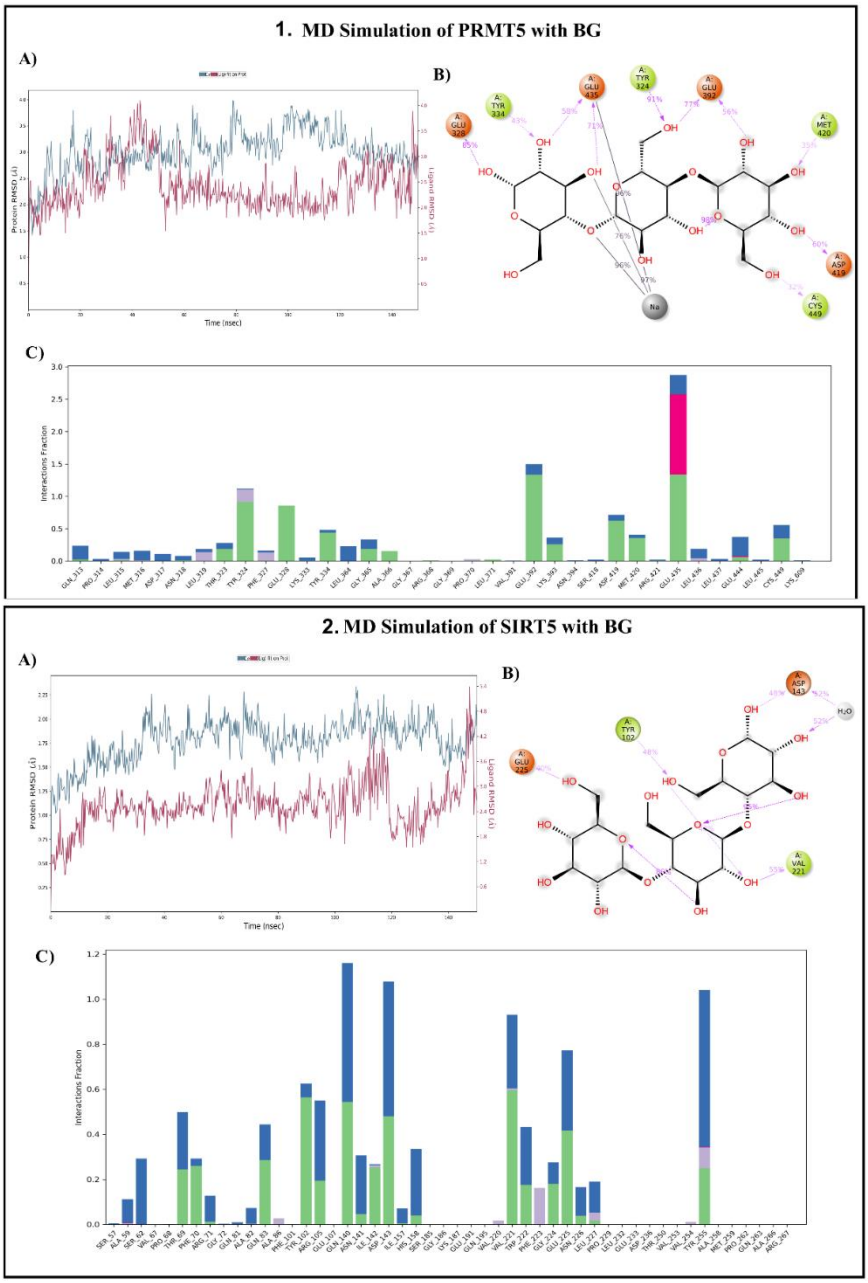

Figure 5. Molecular Dynamics Simulation of **1.** PRMT5-BG and **2.** SIRT5-BG complex: **A)** Root Mean Square Deviation (RMSD) graph, **B)** 2D ligand interactions during simulation with PRMT5 and SIRT5 residues along with % of bonding, **C)** a simulation run of 150 ns showing different bonding interactions of residues with ligand BG (green color: H-bond; blue color: water-bridge interaction; pink color: Ionic; Grey color: hydrophobic interactions). Published in Journal of Biomolecular structure and dynamics, Varsha Virendra Palol et al., 2024.

6.3 *In vitro* cell assessment studies in ovarian cancer

6.3.1 Cell cytotoxicity

The cell cytotoxicity by MTT analysis in OVCAR-3 and SKOV-3 showed that both BGPC and EGPC IC_{50} were within 25-50 µg/mL, while BG and EG exhibited very less cytotoxicity till 100 µg/mL. However, no cell death was observed in normal HEK293 cells. The cytotoxicity was also checked against standard drugs, Cyclophosphamide, Avastin and Valproic acid (39).

No toxicity was observed in NPs treated at 24h and 48h. Cyclophosphamide (CPA) is a standard drug used in the treatment of advanced stages and recurrent OC. CPA is resistant in OVCAR-3 while its effective activity was seen in SKOV-3 cells. Avastin (AVA), a well-known anti-VEGF used in the treatment of OC at stages III and IV in combination with carboplatin and paclitaxel. Its activity is well studied in OVCAR-3; however, it was resistant to SKOV-3. Valproic acid (VPA) is a Histone deacetylase inhibitor. It has a short fatty acid chain. VPA plays a major role in epigenetic modifications with PRMTs and SIRTs. Thus, effective cytotoxicity of BGPC, EGPC along with CPA, AVA and VPA was seen in OVCAR-3 and SKOV-3, respectively (Figure 6A).

6.3.2 Live/dead staining by AO/EB

Acridine orange is a nucleic acid stain that helps in determining viable cells in the cytoplasm and nucleus, while ethidium orange stains the dead cells. Figure 6B shows signs of early and late apoptosis in OVCAR-3 and SKOV-3. The control cells appear green with epithelial structures with no signs of apoptosis. The cells showed changes in the morphology of BGPC and EGPC. In the case of OVCAR-3, the BGPC showed only 30% live cells, and EGPC showed 20%, in comparison to BG and EG, which showed 60% and 50%, respectively. In SKOV-3, both BGPC and EGPC were found to have less than 20% live cells while BGPC and EGPC showed 50% live cells. This shows the effectiveness of NPs in apoptotic activity.

6.3.3 FITC/DAPI analysis

The cytoplasmic/ nuclear staining by FITC/DAPI showed characteristic features of cell elongation and nucleus abnormality in shape. In OVCAR-3, both BGPC and EGPC showed constrained nuclei and cytoplasm when compared to BG and EG extract. BGPC and EGPC showed a significant increase in the fluorescent intensity compared to the nucleus of control. The cytoplasmic/nuclear staining of BGPC and EGPC showed signs of elongated cytoplasm and distressed nuclei in both OVCAR-3 and SKOV-3 cells. While in SKOV-3, the cytoplasmic regions showed signs of blebbing and elongation in BGPC and EGPC, determining the signs of stress during treatment. EG showed a curved nucleus structure. BGPC and EGPC showed higher apoptotic activity (Figure 6C).

6.3.4 Oxidative stress by DCFH-DA

The ROS activity of BGPC and EGPC shows signs of oxidative stress, which contributes to a major part of the cellular process. The derived NPs BGPC and EGPC showed cell blebbing and deformation which denotes signs of oxidative stress. This was absent in BG and EG-treated cells of OVCAR-3; however, in SKOV-3, signs of stress were observed in BG and EG also (Figure 6D).

6.3.5 Wound healing

Wound healing assay was performed to investigate the effects of NPs on ovarian cancer cell migration. The results indicated that the control cells did not exhibit any inhibition of cell migration after 48 h incubation. However, after 48h treatment with BG, EG, BGPC and EGPC, a dose-dependent inhibition of OVCAR-3 and SKOV-3 cancer cell migration was observed. The number of cells that migrated into the scratched area was photographed before and after

drug treatment, at 0 and 48h. It was observed that the BGPC & EGPC effectively inhibited the migration of cells by 50% when compared to BG & EG in both OVCAR-3 and SKOV-3. However, an increased inhibition was seen in EG in OVCAR-3 (Figure 7A).

6.3.6 Cell cycle analysis

The effect of NPs on cell cycle phase distribution was observed by flow cytometry using the PI solution. The treatment of BGPC and EGPC in OVCAR-3 & SKOV-3 showed major arrest in the G1 phase, which shows the cell proliferation stage was halted (Figure 7B). It could be noted that both BG& EG in SKOV-3 showed the absence of the G2M phase with increased inhibition in the S phase when compared to BGPC and EGPC. It was reported that G1 phase cyclins and cyclin-dependent kinases (CDKs) were found to be regulated by PI3K/AKT/mTOR signalling in ovarian cancer (40). Thus, the inhibition of the G1 phase by the NPs shows a major effect on cell proliferation mechanism.

6.3.7 3D spheroids cytotoxicity

The 3D spheroids cytotoxicity was analyzed in both OVCAR-3 and SKOV-3 to analyse the release mechanism of NPs in targeting these cancer cells. The treatment was ranged from 50-150 μg/mL. A difference in cytotoxic treatment was between both cell lines. The OVCAR-3 formed large loose spheroids, while SKOV-3 formed small and compact spheroids. In OVCAR-3, the spheroids were found to dissociate upon increasing concentration in a dose-dependent manner, which resulted in increased diameter of cells upon treatment with BG, EG, BGPC and EGPC. In the case of SKOV-3, the spheroids were found to decrease in size with increasing concentration. Thus, upon treatment, the diameter of SKOV-3 spheroids was found to be reduced in a dose-dependent manner (Figure 8A). In comparison to 2D, the 3D spheroids showed increased cytotoxicity at 100 and 150 μg/mL. The images were photographed after treatment of 48h with phase contrast microscopy and the % size diameter of spheroids was determined by ZEN software.

6.3.8 AO/EB in 3D spheroids

The live/dead staining by AO/EB was performed to check the apoptotic activity of NPs in 3D spheroids. In OVCAR-3, the BGPC and EGPC show major signs of apoptosis with cell death and deeper penetration into the cell in comparison to BG and EG. In SKOV-3, cell death was majorly seen on the outer surface of the spheroid and less penetration was observed (Figure 8B). The AO/EB analysis shows how NPs release mechanism works by targeting differently in both cell lines. The SKOV-3 has rapid migrative properties, while OVCAR-3 has been considered clinically more aggressive, defining how, at different stages, the cell lines acquired can show an impact. Thus, the effect of NPs shows apoptotic effects in the treatment of ovarian cancer.

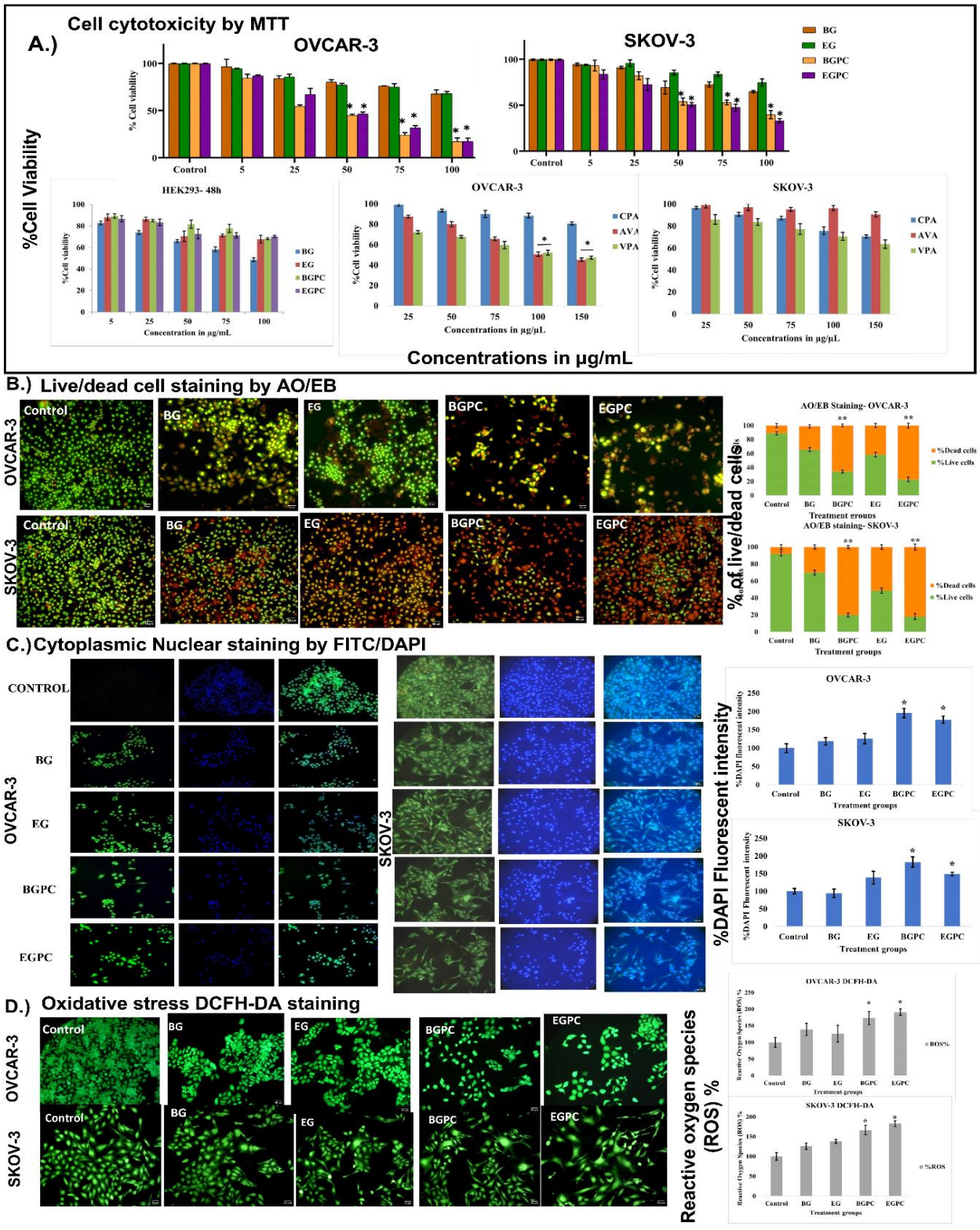

Figure 6 A.) Cell cytotoxicity graphs by MTT upon treatment with control, BG, EG, BGPC and EGPC for 48h in OVCAR-3, SKOV-3 and HEK293T cells. **B.)** Live/dead staining by AO/EB upon treatment for 48h in OVCAR-3 and SKOV-3. **C.)** Cytoplasmic/ nuclear staining by FITC/DAPI upon treatment for 48h in OVCAR-3 and SKOV-3. **D.)** Oxidative stress analysis by DCFH-DA upon treatment for 48h in OVCAR-3 and SKOV-3. Data were presented as the mean ± standard deviation (n = 6). * denotes $p<0.05$; ** denotes $p<0.01$; significance.

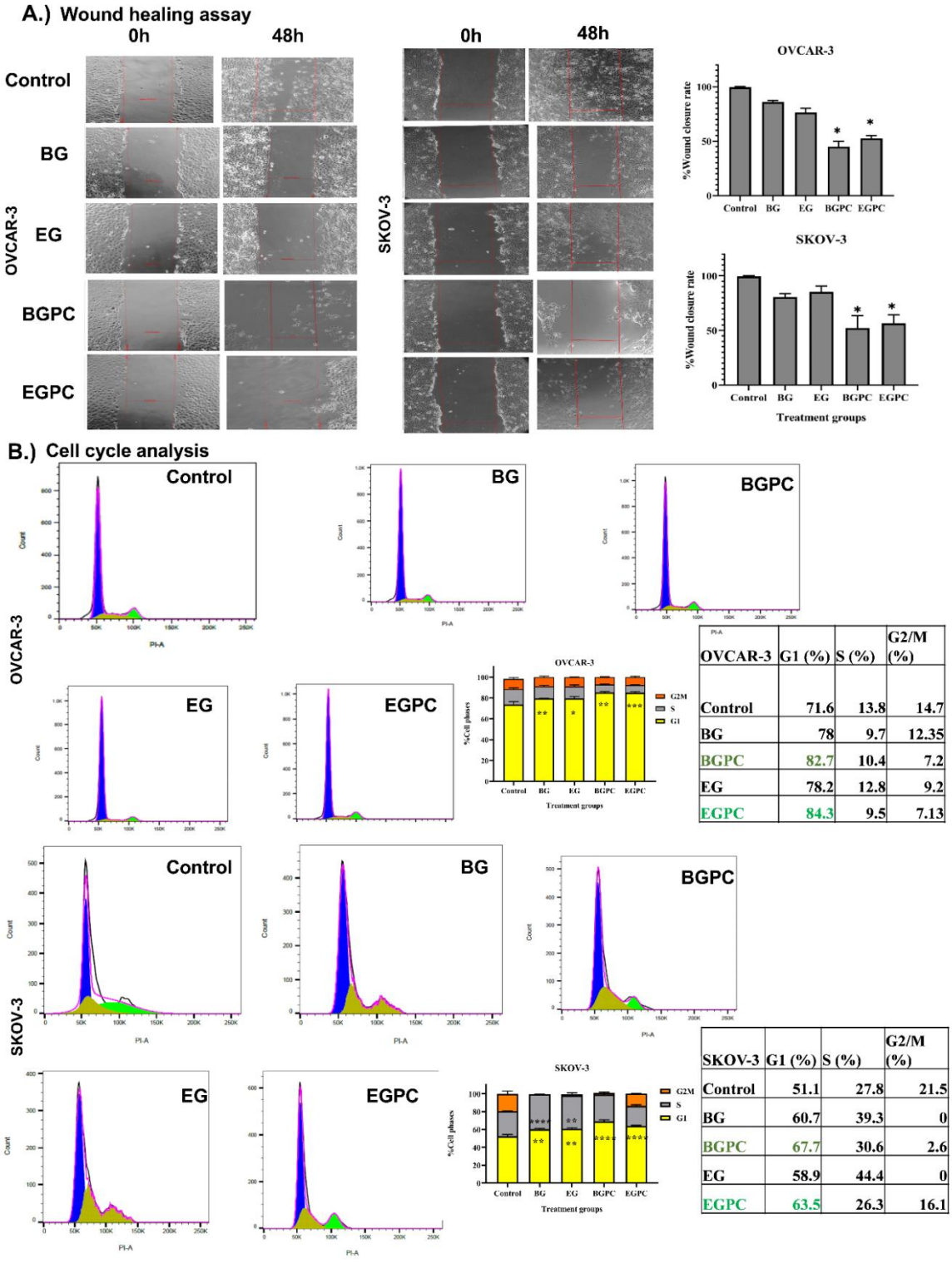

OVCAR-3	G1 (%)	S (%)	G2/M (%)
Control	71.6	13.8	14.7
BG	78	9.7	12.35
BGPC	82.7	10.4	7.2
EG	78.2	12.8	9.2
EGPC	84.3	9.5	7.13

SKOV-3	G1 (%)	S (%)	G2/M (%)
Control	51.1	27.8	21.5
BG	60.7	39.3	0
BGPC	67.7	30.6	2.6
EG	58.9	44.4	0
EGPC	63.5	26.3	16.1

Figure 7 A.) Wound healing in OVCAR-3 & SKOV-3 cells were observed at 0h and 48h with β-1,3-glucan (BG), *Euglena* extract (EG), NPs of β-1,3-glucan (BGPC) and *Euglena gracilis* (EGPC) at IC_{50} concentration at 20X. Data were presented as the mean ± standard deviation (n = 6). **B.)** Cell cycle analysis of different groups treated in OVCAR-3 and SKOV-3 by flow cytometry. Graphical representation of each cell phase arrest % in different treatment groups with control. Data were presented as the mean ± standard deviation (n = 3). * denotes $p<0.05$; ** denotes $p<0.01$; *** denotes $p<0.001$ significance.

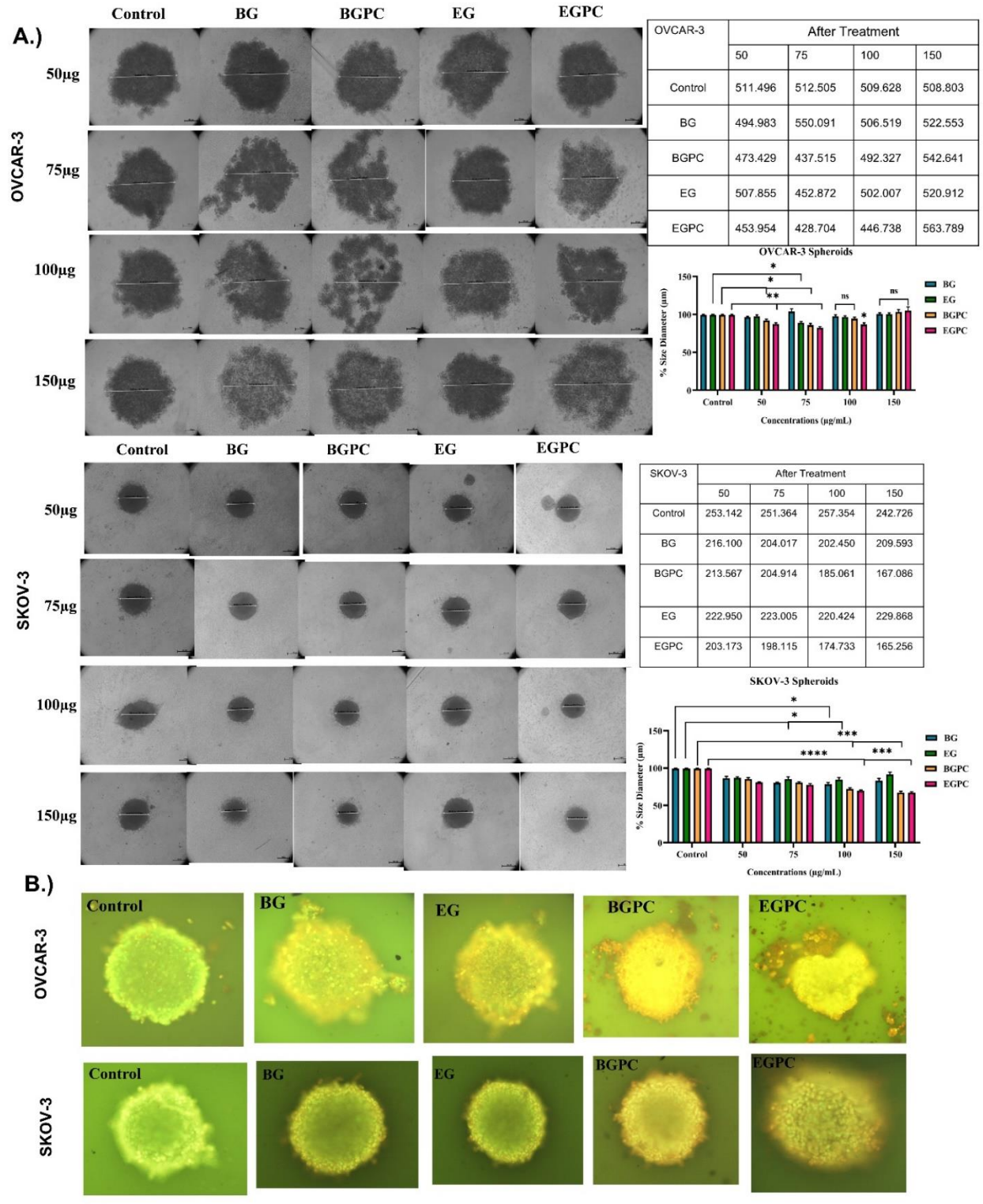

OVCAR-3	After Treatment			
	50	75	100	150
Control	511.496	512.505	509.628	508.803
BG	494.983	550.091	506.519	522.553
BGPC	473.429	437.515	492.327	542.641
EG	507.855	452.872	502.007	520.912
EGPC	453.954	428.704	446.738	563.789

SKOV-3	After Treatment			
	50	75	100	150
Control	253.142	251.364	257.354	242.726
BG	216.100	204.017	202.450	209.593
BGPC	213.567	204.914	185.061	167.086
EG	222.950	223.005	220.424	229.868
EGPC	203.173	198.115	174.733	165.256

Figure 8 A.) Phase contrast microscopic images of OVCAR-3 and SKOV-3 spheroid culture in ULA with different concentrations from 50- 150 µg/mL of treatment groups BG, BGPC, EG and EGPC along with non- treated control (10X objective, scale bar = 100 µm). Graphical Data were presented as the mean ± standard deviation (n = 6). * denotes $p<0.05$; ** denotes $p<0.01$ significance; ns: non-significant. **B.)** Fluorescent microscopic images of OVCAR-3 and SKOV-3 spheroid culture in ULA with treatment groups BG, BGPC, EG and EGPC along with non- treated control (20X objective).

6.4 Effect of the NPs on the Gene expression analysis

In case of OVCAR-3, NRF-2 levels show both BGPC and EGPC were found to be significant at 24 and 48h. The fold change of PRMT4 & 5 shows both BGPC and EGPC significant changes. BG showed elevated changes in PRMT5 at 48h. In case of SIRT1 & 5, both BGPC and EGPC were found to be substantial. EG levels were found to be elevated at 24h, while in SIRT5 BG levels were absent at 24h and elevated at 48h.The pro-apoptotic proteins Caspase 3, 8 and BAD show elevated BGPC and EGPC at both 24 and 48h. The anti-apoptotic activity of BCL-2 show BGPC and EGPC were found to be significant at 48h.The PI3K/AKT/mTOR show the BGPC and EGPC lower levels at 48h showing signs of prominent inhibition of cell proliferation, migration and chemotherapy resistance. However, BG showed no expression in mTOR at both 24 and 48h. In case of MMP-3, BG showed no expression at both 24 and 48h; while EG was expressed at 48h and not in 24h. Both BGPC and EGPC showed significant changes at 48h. While in case of E2F-1 & IL-6, both the conditions, BGPC and EGPC showed similar significant changes at both 24 and 48h. EG was found to be elevated at 24h (Figure 9).

In case of SKOV-3, NRF-2 levels in both BGPC and EGPC were found to be significant at 24 and 48h. The fold change of PRMT4 & 5 in both BGPC and EGPC shows significant changes. BG & EG showed elevated changes in PRMT4 at 24h; while EG was only elevated at 24h in PRMT5. The changes in SIRT1 & 5 shows both BGPC and EGPC found to be significant. BG levels were found to be elevated at 24h, while in SIRT5 BGPC levels were also elevated at 24h. The pro-apoptotic proteins Caspase 3, 8 and BAD show elevated BGPC and EGPC at both 24 and 48h. In BAD, BG was also elevated at 48h. The anti-apoptotic BCL-2 activity of BGPC and EGPC was found to be significant at 48h. The PI3K/AKT/mTOR pathway shows BGPC and EGPC lower levels at 48h showing signs of prominent inhibition of cell proliferation, migration and chemotherapy resistance. However, BG showed a 2.5-fold increased expression in PI3K at 24h. In the case of MMP-3, EG was found to be elevated at 24h. Both BGPC and EGPC showed significant changes at 48h. While, in E2F-1 & IL-6 both conditions show BGPC and EGPC similar significant changes at both 24 and 48h. Both BG & EG were found to be elevated at 24h in E2F-1, while in IL-6, BG expression was absent at 24h (Figure 10).

From the gene expression studies, both BGPC and EGPC showed significant changes across all the markers. This determines their overall drug delivery mechanism in regulating the biological systems by targeting several pathways. The pro-apoptotic markers showed varied expression among OVCAR-3 and SKOV-3 which indirectly affected the expression of epigenetic markers. Oxidative stress among both the cell lines was found to be in similar range. The IL-6 and MMP-3 expression were varying among both the cell lines as one activation leads to another deactivation. The cell proliferation markers showed characteristics with decreased expression over time of 48h. Several changes were observed among both the cell lines from the time span of 24 to 48h of treatment. Both BGPC and EGPC have shown effective changes and contributed to the treatment of ovarian cancer.

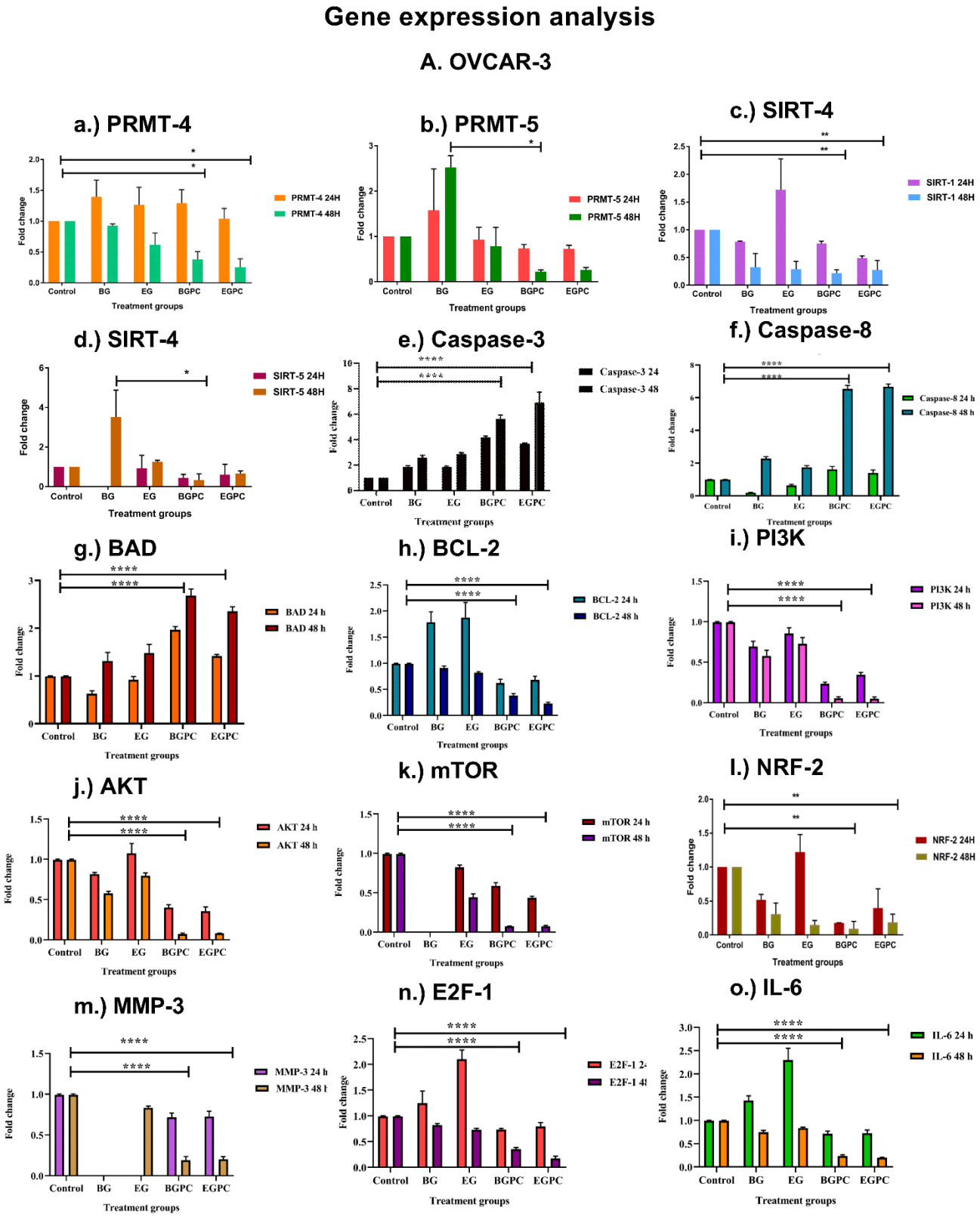

Figure 9. Graphical representation of gene expression analysis from (a. to o.) in OVCAR-3 cells. The cells upon treatment at IC_{50} concentration with treatment groups- Control, β-1,3-glucan (BG), *Euglena* extract (EG), β-1,3-glucan NP (BGPC), *Euglena* NP (EGPC) were analysed by Real-time PCR. * denotes $p<0.05$; ** denotes $p<0.01$, **** denotes $p<0.0001$ when compared with control (n=6).

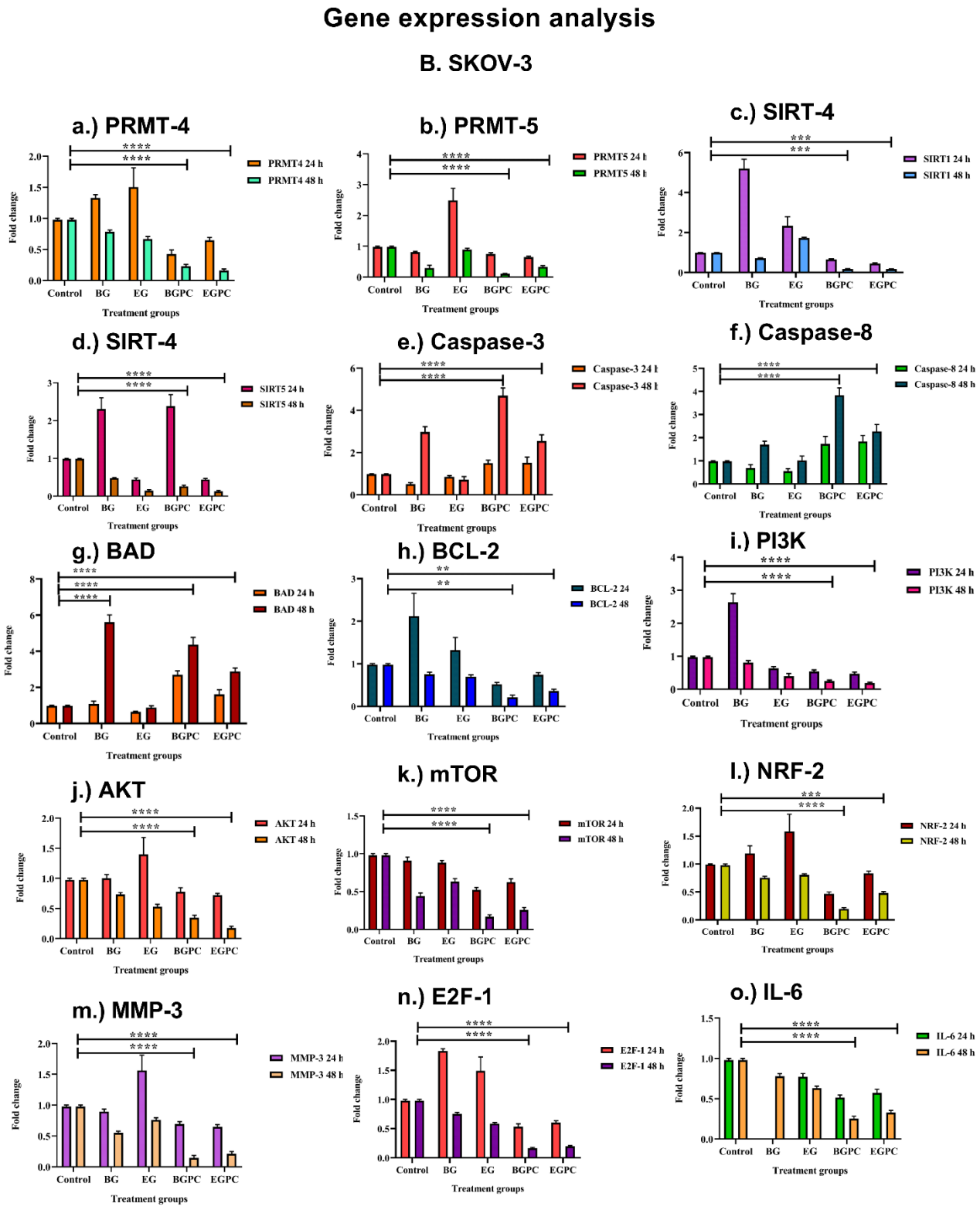

Figure 10. Graphical representation of gene expression analysis from a.) to o.) in SKOV-3 cells. The cells upon treatment at IC_{50} concentration with treatment groups- Control, β-1,3-glucan (BG), *Euglena* extract (EG), β-1,3-glucan NP (BGPC), *Euglena* NP (EGPC) were analysed by Real-time PCR. * denotes $p<0.05$; ** denotes $p<0.01$, **** denotes $p<0.0001$ when compared with control (n=6).

6.5 Effect of NPs on protein analysis by Immunofluorescence and ELISA.

6.5.1 Immunofluorescence studies

The Immunofluorescence influence of NPs on proteins NRF-2, NFκB, β-catenin, E-cadherin and Vimentin was studied in ovarian cancer. The cells were treated with IC_{50} concentration for 48h and the captured fluorescent images were then calculated by CTCF intensity in Image J software (Figure 11A).

NRF-2 plays a major role in oxidative stress and shows high levels in ovarian cancer. In the case of both OVCAR-3 and SKOV-3, the BGPC and EGPC show reduced CTCF intensity when compared with BG and EG which were found to be significant when compared with the control. This shows how NPs are involved in oxidative stress mechanisms with major signs of cell blebbing and change in nucleus shape. To study the inflammation of the cells treated, NFκB protein was used. As NFκB has been found to be in a pro-inflammatory process, it acts as a tumour promoter and is upregulated in ovarian cancer. In the case of OVCAR-3, the BG levels were found to be lower than BGPC, while EGPC was found to be significant in comparison to control. In SKOV-3, the BGPC and BG levels were found to be in a similar range, while EGPC levels were reduced. This could possibly be due to the mechanism of invasion as BGPC and BG were found to be on the same levels. However, an intent target of activation was observed in EGPC in both cell lines. β-catenin protein was studied to understand the cell proliferation and differentiation process. They play a major role in apoptosis and defining cancer stemness, which plays a crucial role in treatment therapeutic options. The levels of both BGPC and EGPC were found to be low when compared to those of the control. These results also correlate with the *in vitro* cell proliferation and apoptotic assays which showed reduced activity of NPs. Thus, the treated cells by NPs could possibly undergo β-catenin signalling process to inhibit the cell differentiation process.

The EMT markers E-cadherin and Vimentin has been associated with cell adhesion and cell invasion respectively. E-cadherin levels were found to be downregulated in ovarian cancer. However, Vimentin was found absent in the benign stage, yet it has been expressed in advanced stages. In our study, the E-cadherin levels of BGPC and EGPC were found to be upregulated in both OVCAR-3 and SKOV-3. However, EGPC levels in OVCAR-3 were not found to be significant. Vimentin is not expressed in OVCAR-3, and the NPs treated showed increased levels of vimentin. However, in the case of SKOV-3, vimentin is expressed, and thus, the NPs represent the lower levels. Vimentin is a type of intermediate filament and thus is involved in the rapid migration process, which has been found in SKOV-3, while OVCAR-3 was found to be aggressive. The migration ability is limited, which was observed in 3D spheroids. This defines the role of protein at different stages of cancer depending on the cell type and proliferation. Overall, the NPs BGPC and EGPC showed positive characteristics in all of the proteins, showing their potency to combat multiple signalling pathways in OC. The epigenetic markers were also governed by these proteins in the cellular process which indirectly affects the activation process. Thus, BGPC and EGPC show prominent drug delivery characteristics in overcoming OC (Figure 11A).

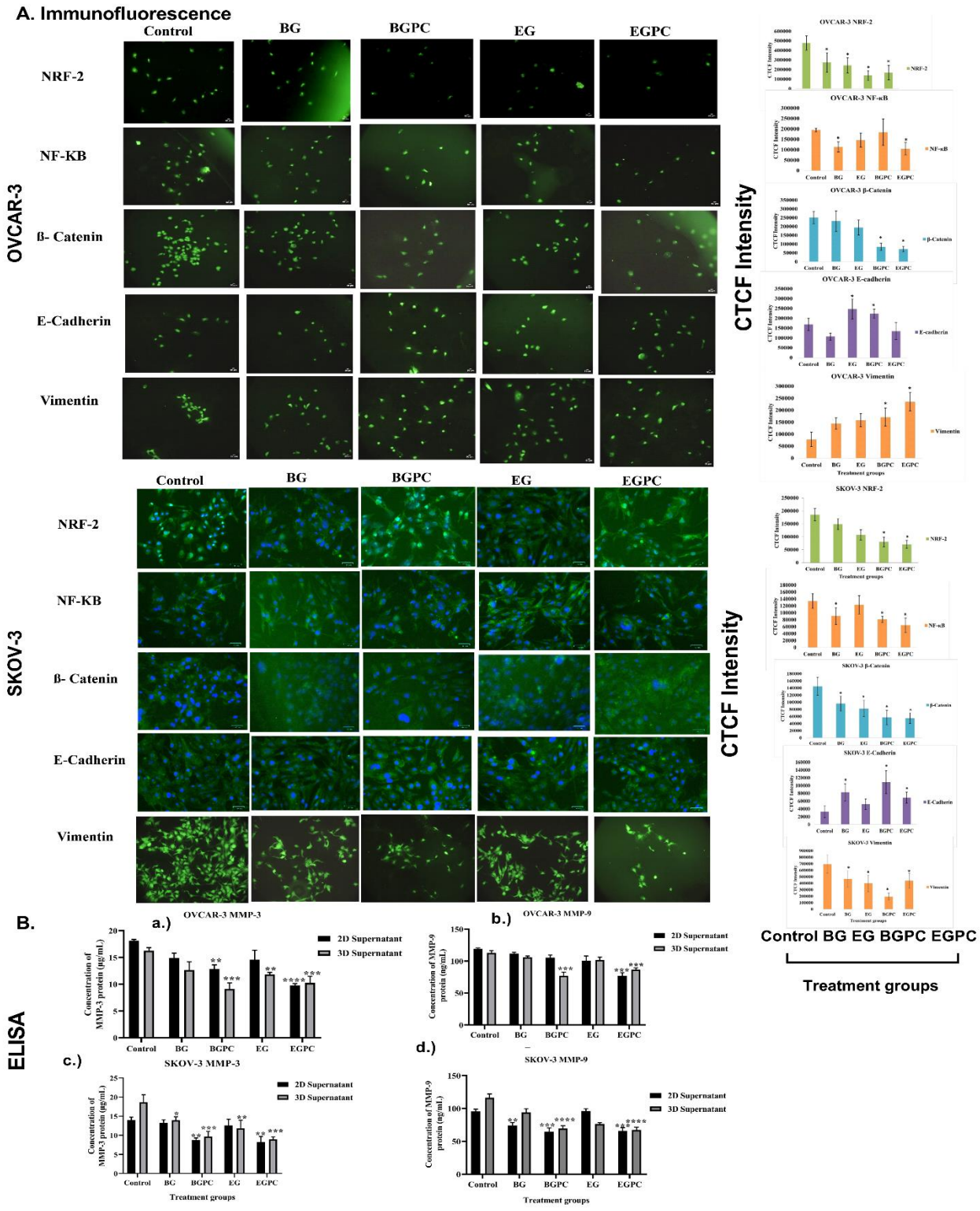

Figure 11 A. Immunofluorescence of proteins NRF-2, NFκB, β-catenin, E-cadherin, Vimentin in OVCAR-3 and SKOV-3 cells at IC_{50} for 48h in 20X with scale 40µm. Histographic representation of % CTCF intensity of Immunofluorescent stain/ DAPI stains nucleus analysed by Image J software. Data were presented as the mean ± standard deviation (n = 6). **B.** ELISA graphs of MMP-3 and MMP-9 with treatment groups of 2D and 3D cell culture supernatant of a.) & b.) OVCAR-3 and c.) & d.) SKOV-3. Data were presented as the mean ± standard deviation (n = 2). * denotes $p<0.05$; ** denotes $p<0.01$; *** denotes $p<0.001$ and **** denotes $p<0.0001$ significance when compared with control.

6.5.2 ELISA analysis

ELISA analysis for MMP-3 and 9 was performed for 2D and 3D culture-treated supernatants in OVCAR-3 and SKOV-3. The Matrix Metalloproteases (MMPs) are associated with collagen degradation in OC. MMP-3 and 9 were widely studied for tumour invasion and metastasis. Both MMP-3 and 9 degrade E-cadherin providing less functionality to the cell. MMP-9 acts as a potential serum biomarker for OC diagnosis. The MMP-3 and 9 were found to be upregulated in OC. MMP-3&9 levels in OVCAR-3 and SKOV-3 showed lower levels when treated with NPs BGPC and EGPC. No significance was observed between 2D and 3D culture supernatants. However, the levels in treated NPs were found to be significant in comparison to control in both 2D and 3D levels of OVCAR-3 and SKOV-3 (Figure 11B). In several recent studies, MMPs were a major therapeutic target, and several inhibitors have been developed for target specification. Thus, based on the invasion ability of NPs as observed in wound healing, the NPs were found to target the MMPs effectively signifying their major role in the invasion process of OC.

7. SUMMARY AND CONCLUSION

The NPs from β-1,3-glucan and *Euglena gracilis* was studied for drug delivery in combating ovarian cancer. The developed NPs were characterized based on size, shape, nature and HRLC-MS/MS characterization which were found to be optimum for drug delivery. The size of the NPs BGPC and EGPC were found to be 134.62 nm and 158.38 nm respectively. The synthesied NPs were further investigated on the epigenetic regulation in OC. For which a pilot understanding of major compound BG known for its several biological properties was analyzed *in silico* by epigenetic targets PRMTs and SIRTs, among which PRMT5 and SIRT5 were found to be more prominent with molecular simulation studies. The cytotoxicity, apoptotic, wound healing and cell cycle analysis of the NPs developed, show prominent characteristics by inhibiting cell proliferation and apoptosis. The IC_{50} of BGPC and EGPC was found to be between 25-50 µg/mL in both OVCAR-3 and SKOV-3, when compared with the non-derived forms BG and EG which exhibited IC_{50} >100 µg/mL. The wound healing assay inhibited migration property of BGPC and EGPC by 50% when compared to that of control. To further analyse the effectiveness of NPs, an *in vivo* mimicking model was proposed in 3D spheroids to check NPs mechanism for cell invading process. The 3D spheroids signified the delivery mechanism of NPs in both OVCAR-3 and SKOV-3 which showed distinct characteristics of cell cytotoxicity and apoptosis affecting the tumour microenvironment. The spheroid of OVCAR-3 was loose in nature, and SKOV-3 was compact in nature. The both NPs BGPC and EGPC exhibited prominent invading activity at 75-150 µg/mL by dissociating the spheroids in OVCAR-3, while in SKOV-3 reduction in the overall size of the spheroids was observed when compared to BG and EG. The cell cycle analysis of BGPC and EGPC in OVCAR-3 & SKOV-3 showed major arrest in the G1 phase, which shows the cell proliferation stage, was halted. The NPs impact on the apoptotic, oxidative stress and inflammatory markers in OC cell lines at different time frames of 24 and 48h of treatment showed prominent effect on the cellular process. Both BGPC and EGPC exhibited profound apoptotic, inflammatory and cell proliferation activity which majorly impacted on the epigenetic markers PRMT4,5 and SIRT1,5 with a statistical significance of

$p<0.05$. The NRF-2, NFκB, E-cadherin, β- Catenin and Vimentin properties influenced by NPs show their integral part in the biological system where the epigenetic markers PRMT4,5 and SIRT1,5 were predisposed by the similar cellular process. The MMP3 and MMP9 activity by NPs showed reduced levels of BGPC and EGPC in 2D and 3D cultures which influence the migratory property and collagen degradation state in OC cells. Thus, from the current study, the developed NPs exhibit efficient cell invading properties *in vitro* in 2D and 3D *in vivo* mimicking model. The NPs represent efficient drug delivery properties in physical and biological systems with major influence on the epigenetic factors in combating OC with diverse signalling mechanisms.

8. ABSTRACT

Background: Nanophytosomes (NPs) are novel lipid vesicular drug delivery systems known for formulating herbal extracts for better absorption and bioavailability. *Euglena gracilis* (EG), a unicellular alga rich in β-1,3 glucan (BG), exhibits biological and anti-cancer properties. The utilization of BG and EG extract as NPs holds promise for efficient drug delivery characteristics. This study focuses on epigenetic modulators, Protein Arginine Methyltransferases (PRMTs), and Sirtuins (SIRTs), with a key role of NPs involved in combating ovarian cancer.

Methods: The NPs were synthesized by solvent evaporation and characterized by DLS, FTIR, XRD, HRLC-MS/MS, SEM, and TEM. *In silico* analysis of PRMTs and SIRTs was performed by Glide and Desmond software. OVCAR-3 and SKOV-3 cell lines were used for cytotoxicity, wound healing, cell cycle analysis, gene expression analysis, protein immunofluorescence, and ELISA studies.

Results: The effective NPs BGPC and EGPC were spherical, with 134.62nm and 158.38nm, respectively. They elicit cytotoxicity against OVCAR-3 & SKOV-3 in both 2D & 3D models. The gene expression analysis of BGPC and EGPC has shown regulation of epigenetic markers PRMT4,5 and SIRT1,5 with apoptosis, inflammatory, oxidative stress with a significance of $p<0.01$. The protein immunofluorescence studies of BGPC and EGPC showed effectivity against markers NRF-2, NFκB, β- catenin, E-cadherin, and Vimentin with a significance of $p<0.05$. ELISA analysis of MMP-3&9 exhibited reduced levels of NPs in 2D and 3D cultures. The NPs potentially influence the epigenetic markers via cytoplasmic, nuclear, and mitochondrial activity by several cellular processes.

Conclusion: The BGPC and EGPC were found to be promising candidates for the treatment strategy of ovarian cancer.

9. REFERENCES

1. SEER [Internet]. [cited 2020 Oct 21]. Cancer of the Ovary - Cancer Stat Facts. Available from: https://seer.cancer.gov/statfacts/html/ovary.html

2. Mathur P, Sathishkumar K, Chaturvedi M, Das P, Sudarshan KL, Santhappan S, et al. Cancer Statistics, 2020: Report From National Cancer Registry Programme, India. JCO Glob Oncol [Internet]. 2020 Jul 16 [cited 2022 Aug 1];6:GO.20.00122.

3. Li Y, Gao Y, Zhang X, Guo H, Gao H. Nanoparticles in precision medicine for ovarian cancer: From chemotherapy to immunotherapy. International Journal of Pharmaceutics [Internet]. 2020 Dec 15 [cited 2022 Aug 2];591:119986.

4. Pantshwa JM, Kondiah PPD, Choonara YE, Marimuthu T, Pillay V. Nanodrug Delivery Systems for the Treatment of Ovarian Cancer. Cancers (Basel) [Internet]. 2020 Jan 15 [cited 2022 Oct 19];12(1):213.

5. Barani M, Sangiovanni E, Angarano M, Rajizadeh MA, Mehrabani M, Piazza S, et al. Phytosomes as Innovative Delivery Systems for Phytochemicals: A Comprehensive Review of Literature. Int J Nanomedicine [Internet]. 2021 Oct 15 [cited 2022 Oct 19];16:6983–7022.

6. Yao Y, Zhou Y, Liu L, Xu Y, Chen Q, Wang Y, et al. Nanoparticle-Based Drug Delivery in Cancer Therapy and Its Role in Overcoming Drug Resistance. Frontiers in Molecular Biosciences [Internet]. 2020 [cited 2022 Oct 19];7.

7. Gohari Mahmoudabad A, Gheybi F, Mehrabi M, Masoudi A, Mobasher Z, Vahedi H, et al. Synthesis, characterization and hepatoprotective effect of silymarin phytosome nanoparticles on ethanol-induced hepatotoxicity in rats. Bioimpacts [Internet]. 2023 [cited 2024 Oct 13];13(4):301–11.

8. Mirhafez SR, Azimi-Nezhad M, Dehabeh M, Hariri M, Naderan RD, Movahedi A, et al. The Effect of Curcumin Phytosome on the Treatment of Patients with Non-alcoholic Fatty Liver Disease: A Double-Blind, Randomized, Placebo-Controlled Trial. Adv Exp Med Biol. 2021;1308:25–35.

9. Sugiyama A, Hata S, Suzuki K, Yoshida E, Nakano R, Mitra S, et al. Oral administration of paramylon, a beta-1,3-D-glucan isolated from Euglena gracilis Z inhibits development of atopic dermatitis-like skin lesions in NC/Nga mice. J Vet Med Sci. 2010 Jun;72(6):755–63.

10. Watanabe T, Shimada R, Matsuyama A, Yuasa M, Sawamura H, Yoshida E, et al. Antitumor activity of the β-glucan paramylon from Euglena against preneoplastic colonic aberrant crypt foci in mice. Food Funct. 2013 Nov;4(11):1685–90.

11. Suzuki K, Nakashima A, Igarashi M, Saito K, Konno M, Yamazaki N, et al. Euglena gracilis Z and its carbohydrate storage substance relieve arthritis symptoms by modulating Th17 immunity. PLoS ONE. 2018;13(2):e0191462.

12. Sugiyama A, Suzuki K, Mitra S, Arashida R, Yoshida E, Nakano R, et al. Hepatoprotective effects of paramylon, a beta-1, 3-D-glucan isolated from Euglena gracilis Z, on acute liver injury induced by carbon tetrachloride in rats. J Vet Med Sci. 2009 Jul;71(7):885–90.

13. Shimada R, Fujita M, Yuasa M, Sawamura H, Watanabe T, Nakashima A, et al. Oral administration of green algae, Euglena gracilis, inhibits hyperglycemia in OLETF rats, a model of spontaneous type 2 diabetes. Food Funct. 2016 Nov 9;7(11):4655–9.

14. Tomiyama T, Goto K, Tanaka Y, Maruta T, Ogawa T, Sawa Y, et al. A major isoform of mitochondrial trans-2-enoyl-CoA reductase is dispensable for wax ester production in Euglena gracilis under anaerobic conditions. PLOS ONE [Internet]. 2019 Jan 16 [cited 2020 Feb 28];14(1):e0210755.

15. Ishiguro S, Upreti D, Robben N, Burghart R, Loyd M, Ogun D, et al. Water extract from Euglena gracilis prevents lung carcinoma growth in mice by attenuation of the myeloid-derived cell population. Biomedicine & Pharmacotherapy [Internet]. 2020 Jul 1 [cited 2020 Oct 9];127:110166.

16. Al-Alem LF, Baker AT, Pandya UM, Eisenhauer EL, Rueda BR. Understanding and Targeting Apoptotic Pathways in Ovarian Cancer. Cancers (Basel) [Internet]. 2019 Oct 24 [cited 2024 Oct 12];11(11):1631.

17. Singh A, Srivastav S, Singh MP, Singh R, Kumar P, Kush P. Recent advances in phytosomes for the safe management of cancer. Phytomedicine Plus [Internet]. 2024 May 1 [cited 2024 Nov 4];4(2):100540.

18. Ediriweera MK, Tennekoon KH, Samarakoon SR. Role of the PI3K/AKT/mTOR signaling pathway in ovarian cancer: Biological and therapeutic significance. Seminars in Cancer Biology [Internet]. 2019 Dec 1 [cited 2024 Oct 12];59:147–60.

19. Teng CF, Yu CH, Chang HY, Hsieh WC, Wu TH, Lin JH, et al. Chemopreventive Effect of Phytosomal Curcumin on Hepatitis B Virus-Related Hepatocellular Carcinoma in A Transgenic Mouse Model. Sci Rep. 2019 Jul 17;9(1):10338.

20. Tossetta G, Marzioni D. Natural and synthetic compounds in Ovarian Cancer: A focus on NRF2/KEAP1 pathway. Pharmacological Research [Internet]. 2022 Sep 1 [cited 2024 Oct 12];183:106365.

21. Sabzichi M, Hamishehkar H, Ramezani F, Sharifi S, Tabasinezhad M, Pirouzpanah M, et al. Luteolin-loaded phytosomes sensitize human breast carcinoma MDA-MB 231 cells to doxorubicin by suppressing Nrf2 mediated signalling. Asian Pac J Cancer Prev. 2014;15(13):5311–6.

22. Al-Alem L, Curry TE. Ovarian cancer: involvement of the matrix metalloproteinases. Reproduction [Internet]. 2015 Aug [cited 2024 Oct 13];150(2):R55–64.

23. Barani M, Sangiovanni E, Angarano M, Rajizadeh MA, Mehrabani M, Piazza S, et al. Phytosomes as Innovative Delivery Systems for Phytochemicals: A Comprehensive Review of Literature. International Journal of Nanomedicine [Internet]. 2021 Oct 15 [cited 2024 Nov 4];16:6983–7022.

24. Ibrahim A, El-Meligy A, Fetaih H, Dessouki A, Stoica G, Barhoumi R. Effect of curcumin and Meriva on the lung metastasis of murine mammary gland adenocarcinoma. In Vivo. 2010;24(4):401–8.

25. Szulc-Kielbik I, Kielbik M, Nowak M, Klink M. The implication of IL-6 in the invasiveness and chemoresistance of ovarian cancer cells. Systematic review of its potential role as a biomarker in ovarian cancer patients. Biochimica et Biophysica Acta (BBA) - Reviews on Cancer [Internet]. 2021 Dec 1 [cited 2024 Oct 13];1876(2):188639.

26. Rosso M, Majem B, Devis L, Lapyckyj L, Besso MJ, Llauradó M, et al. E-cadherin: A determinant molecule associated with ovarian cancer progression, dissemination and aggressiveness. PLOS ONE [Internet]. 2017 Sep 21 [cited 2024 Oct 13];12(9):e0184439.

27. Marjaneh RM, Rahmani F, Hassanian SM, Rezaei N, Hashemzehi M, Bahrami A, et al. Phytosomal curcumin inhibits tumor growth in colitis-associated colorectal cancer. J Cell Physiol. 2018 Oct;233(10):6785–98.

28. Nguyen VHL, Hough R, Bernaudo S, Peng C. Wnt/β-catenin signalling in ovarian cancer: Insights into its hyperactivation and function in tumorigenesis. J Ovarian Res [Internet]. 2019 Dec 11 [cited 2024 Oct 13];12:122.

29. Zhan L, Zhang Y, Wang W, Song E, Fan Y, Wei B. E2F1: a promising regulator in ovarian carcinoma. Tumor Biol [Internet]. 2016 Mar 1 [cited 2024 Oct 13];37(3):2823–31.

30. YMER2212D5.pdf [Internet]. [cited 2024 Nov 4].

31. Li G, Xu W, Li X, Chen M, Shi Y, Wei M, et al. Oncogenic SIRT7 inhibits GATA4 transcriptional activity and activates the Wnt signaling pathway in ovarian cancer. Gynecologic Oncology [Internet]. 2023 Apr 1 [cited 2024 Feb 10];171:39–48.

32. Kim YS, Gupta Vallur P, Jones VM, Worley BL, Shimko S, Shin DH, et al. Context-dependent activation of SIRT3 is necessary for anchorage-independent survival and metastasis of ovarian cancer cells. Oncogene. 2020 Feb;39(8):1619–33.

33. Poulard C, Corbo L, Le Romancer M. Protein arginine methylation/demethylation and cancer. Oncotarget [Internet]. 2016 Aug 18 [cited 2023 May 2];7(41):67532–50.

34. Palol VV, Saravanan SK, Vuree S, Chinnadurai RK, Subramanyam V. Nanophytosome formulation of β-1,3-glucan and *Euglena gracilis* extract for drug delivery applications. MethodsX [Internet]. 2023 Dec 1 [cited 2024 Oct 13];11:102480.

35. Friesner RA, Murphy RB, Repasky MP, Frye LL, Greenwood JR, Halgren TA, et al. Extra precision glide: docking and scoring incorporating a model of hydrophobic enclosure for protein-ligand complexes. J Med Chem. 2006 Oct 19;49(21):6177–96.

36. Mosmann T. Rapid colorimetric assay for cellular growth and survival: application to proliferation and cytotoxicity assays. J Immunol Methods [Internet]. 1983 Dec 1 [cited 2021 Dec 7];65(1–2):55–63.

37. Roper SJ, Linke F, Scotting PJ, Coyle B. 3D spheroid models of paediatric SHH medulloblastoma mimic tumour biology, drug response and metastatic dissemination. Sci Rep [Internet]. 2021 Feb 19 [cited 2024 Oct 13];11(1):4259.

38. Antonysamy S, Bonday Z, Campbell RM, Doyle B, Druzina Z, Gheyi T, et al. Crystal structure of the human PRMT5:MEP50 complex. Proc Natl Acad Sci U S A [Internet]. 2012 Oct 30 [cited 2023 Jul 3];109(44):17960–5.

39. Effects of Valproic Acid with Different Drugs in Ovarian Cancer Cell Lines: An in vitro Study. Biointerface Res Appl Chem [Internet]. 2022 Jul 10 [cited 2024 Oct 13];13(3):279.

40. Gao N, Flynn DC, Zhang Z, Zhong XS, Walker V, Liu KJ, et al. G1 cell cycle progression and the expression of G1 cyclins are regulated by PI3K/AKT/mTOR/p70S6K1 signaling in human ovarian cancer cells. Am J Physiol Cell Physiol. 2004 Aug;287(2):C281-291.

10. PUBLICATIONS

- **Palol VV**, Saravana S, Subramanyam V, Ganapathy R, Chinnadurai RK, Subramanian B. Effects of Valproic Acid with Different Drugs in Ovarian Cancer Cell Lines: An *in vitro* Study. Biointerface research in applied chemistry. 2022; 13(3):279-292.
- **Palol VV**, Saravanan SK, Vuree S, Chinnadurai RK, Subramanyam V. Nanophytosome formulation of β-1, 3-glucan and *Euglena gracilis* extract for drug delivery applications. MethodsX. 2023 Nov 20:102480.
- **Varsha Virendra Palol**, Kamran Waidha, Balasubramanian Moovarkumudalvan, Navya Valavath Baburajan, Suresh Kumar Saravanan, Divya Lakshmanan, Veni Subramanyam, Raj Kumar Chinnadurai. β-1,3-Glucan from *Euglena gracilis*: A Promising Epidrug Targeting Epigenetic Regulators PRMTs and SIRTs for Therapeutic Applications in Ovarian cancer. Journal of Biomolecular Structure and Dynamics. Accepted 23 Apr 2024 (Under Production)
- **Palol VV**, Saravanan SK, Chinnadurai RK, Subramanyam V. Epigenetic modification: key regulator of reprogramming in cancer stem cells. In Cancer Stem Cells and Signaling Pathways 2024 Jan 1 (pp. 227-242). Academic Press.

11. PODIUM/ POSTER PRESENTATIONS AT INTERNATIONAL CONFERENCE

- **Winner** of **Oral presentation** under Group C at **"5th International Conference on Recent trends in Bioengineering"** conducted by MIT- School of Bioengineering Sciences & Research, MIT-ADT University, Pune (12th – 13th February, 2022).

- Received **first prize in E-poster** titled "Anticancer activity of *Euglena gracilis* derived phytosomes and *Insilico* analysis of epigenetic regulators Protein arginine methyltransferases (PRMTs) and Sirtuins (SIRTs) with 1,3 β-glucan" at *International Virtual Conference on **"Drug Discovery & Translational Research" (DDTR 2021),*** organized by Department of Biochemistry and Molecular Biology, Pondicherry University (25th-26th February, 2021).

MethodsX 11 (2023) 102480

Contents lists available at ScienceDirect

MethodsX

journal homepage: www.elsevier.com/locate/methodsx

Nanophytosome formulation of β-1,3-glucan and *Euglena gracilis* extract for drug delivery applications ☆

Varsha Virendra Palol[a], Suresh Kumar Saravanan[b], Sugunakar Vuree[c], Raj Kumar Chinnadurai[a], Veni Subramanyam[a,*]

[a] Mahatma Gandhi Medical Advanced Research Institute (MGMARI), Sri Balaji Vidyapeeth (Deemed to-be University), Pillayarkuppam, Puducherry 607402, India
[b] Mahatma Gandhi Medical Preclinical Research Centre (MGMPRC), Sri Balaji Vidyapeeth (Deemed to-be University), Pillayarkuppam, Puducherry 607402, India
[c] MNR Foundation for Research and Innovation, MNR Medical College and Hospital, MNR Nagar, Fasalwadi, Narsapur Road, Sangareddy 502294, India

ARTICLE INFO

Method name:
Synthesis of Nanophytosomes

Keywords:
Nanophytosome synthesis
Drug delivery
β-1,3 glucan
Euglena gracilis
Solvent evaporation
Temperature

ABSTRACT

Euglena gracilis (EG) is a unicellular freshwater alga known for its high β-1,3-glucan (BG) content with well-known biological properties and immune response. The high molecular weight structure of BG traditionally poses a challenge in terms of its size and absorption. Therefore, the aim of this study was to develop a novel drug delivery mechanism of BG and EG to nanophytosomes (NPs) by converting the heavy molecular weight of BG and EG into lipid phosphatidylcholine (PC), which plays an important role in improving their bioavailability and entrapment in captivity. The BG and EG NPs were developed by the solvent evaporation method while varying time and temperature to optimize their drug delivery ability. The size of BG-PC and EG-PC obtained by the Dynamic Light Scattering (DLS) method was 134.62 and 158.38 nm, respectively. Chemical (Fourier Transform Infra-Red) and structural (X-Ray Diffraction) characterization of NPs improved the binding capacity and the amorphous nature of both NPs. The shape of the NPs by Scanning electron microscopy (SEM) and Transmission electron microscopy (TEM) revealed their spherical, vesicular nature. The encapsulation efficiency of BG-PC and EG-PC was 82 ± 1.62 % and 87 ± 3.22 %, respectively, which improves the bioavailability. The developed methodology has thus proven effective in synthesizing BG-PC and EG-PC, which may be useful as NP drug delivery carriers. Future research could demonstrate the safety and effectiveness of long-term storage conditions for medical and pharmaceutical applications.

- Nanophytosomes are tailored in size, shape and composition to optimize the delivery of phytochemicals/phytocompounds through nanoscale size and surface modification for better physiological absorption.
- Nanophytosomes increase the stability of phytochemicals/phytocompounds and protect them from degradation due to heat or chemical reactions, leading to longer shelf life and improved therapeutic efficacy.
- In this method, optimal conditions were created for the formation of β-1,3-glucan and *Euglena gracilis* extract nanophytosomes for successful development of drug delivery system that can effectively deliver bioactive compounds.

☆ **Related research article** W. Maryana, H. Rachmawati, D. Mudhakir, Formation of phytosome containing silymarin using thin layer-hydration technique aimed for oral delivery, Mater. Today: Proc. 3(2016) 855-866. 10.1016/j.matpr.2016.02.019

* Corresponding author.
E-mail addresses: vsubramcidrf@gmail.com, venis@mgmari.sbvu.ac.in (V. Subramanyam).

https://doi.org/10.1016/j.mex.2023.102480
Received 31 December 2022; Accepted 8 November 2023
Available online 20 November 2023
2215-0161/© 2023 The Author(s). Published by Elsevier B.V. This is an open access article under the CC BY-NC-ND license (http://creativecommons.org/licenses/by-nc-nd/4.0/)

Biointerface Research in Applied Chemistry
Open-Access Journal (ISSN: 2069-5837)

Article
Volume 13, Issue 3, 2021, 279
https://doi.org/10.33263/BRIAC133.279

Effects of Valproic Acid with Different Drugs in Ovarian Cancer Cell Lines: An *in vitro* Study

Varsha Virendra Palol [1], Sowmi Saravana [2], Veni Subramanyam [1,*], Ramakrishnan Ganapathy [3], Raj Kumar Chinnadurai [3], Balanehru Subramanian [1]

[1] Central Inter-Disciplinary Research Facility (CIDRF), Sri Balaji Vidyapeeth (Deemed to be University), Puducherry-607402, India; maheshwarivarsha00@gmail.com (V.V.P.); vsubramcidrf@gmail.com (V.S); balanehrusbv@gmail.com (B.S.);
[2] Department of Biotechnology, Jeppiaar Engineering College, Chennai, Tamil Nadu-600119, India; sowmijasmin22@gmail.com (S.S.);
[3] Center for Animal Research, Training and Services (CAReTs), CIDRF, Sri Balaji Vidyapeeth (Deemed to be University), Puducherry-607402, India; graman83@gmail.com (R.G); rajkumar128@gmail.com (R.K.C.);
* Correspondence: vsubramcidrf@gmail.com (V.S.);

Scopus Author ID 57204634817
Received: 12.04.2022; Accepted: 16.05.2022; Published: 10.07.2022

Abstract: Ovarian cancer is one of the most lethal malignancies, ranked seventh among all cancers globally. In recent trends, there has been an increased use of natural compounds combined with conventional drugs in clinical trials to combat chemotherapeutic resistance. Valproic acid, a short-chain fatty acid, Resveratrol, Silymarin, and Cyclophosphamide are some of the compounds widely studied for various cancer treatments. Hence, an *in vitro* attempt at the combinatorial effect of drugs was investigated in human ovarian adenocarcinoma cells OVCAR-3 and SKOV-3. Cytotoxicity, apoptosis, and antioxidant scavenging activity were studied by MTT, AO/EB, and DPPH assay, respectively. In addition, analysis of quantitative residual protein of treated cell culture supernatants was evaluated in OVCAR-3 and SKOV-3. The combination of valproic acid with resveratrol and silymarin showed effective IC_{50} and apoptosis when compared with cyclophosphamide. The antioxidant activity of valproic acid in combination with resveratrol and silymarin was 88% and 81%, respectively, at 50µg/ml. The study highlights the effective treatment strategy of combinatorial drugs for ovarian cancer. However, the limitations extend towards a molecular approach in the future for further validation with various other *in vitro* methods and preclinical studies.

Keywords: valproic acid; cytotoxicity; resveratrol; silymarin; ovarian cancer.

© 2022 by the authors. This article is an open-access article distributed under the terms and conditions of the Creative Commons Attribution (CC BY) license (https://creativecommons.org/licenses/by/4.0/).

1. Introduction

Ovarian cancer is a complex neoplastic assembly considered the most lethal gynecological malignancy [1]. According to the survey per year, the rate of women getting new cases of ovarian cancer is 11.2, and the death rate is 6.7 per 100000 women [2]. Numerous chemotherapeutic studies have been done to treat advanced ovarian cancer. Treatment options for high-grade serous carcinoma include chemotherapeutic drugs with increased side effects. The development of chemo-resistance mechanisms has decreased the survival rate, and there is a need for more combinations of drugs with natural compounds to avoid resistance and increase survival with minimal side effects. Natural compounds have been on the market for several years and are replacing conventional drugs in clinical trials [3]. Over the years, combination therapy paved the way for diverse therapeutic strategies. The ancient medicine system has used

JOURNAL OF BIOMOLECULAR STRUCTURE AND DYNAMICS
https://doi.org/10.1080/07391102.2024.2425832

Taylor & Francis
Taylor & Francis Group

Check for updates

β-1,3-glucan from *Euglena gracilis*: a promising epidrug targeting epigenetic regulators PRMTs and SIRTs for therapeutic applications in ovarian cancer

Varsha Virendra Palol[a]*, Kamran Waidha[b]*, Balasubramanian Moovarkumudalvan[a], Navya Valavath Baburajan[c], Suresh Kumar Saravanan[d], Divya Lakshmanan[a], Veni Subramanyam[a], and Raj Kumar Chinnadurai[a]

[a]Mahatma Gandhi Medical Advanced Research Institute (MGMARI), Sri Balaji Vidyapeeth (Deemed to-be University), Pillayarkuppam, Puducherry, India; [b]The Shraga Segal Department of Microbiology, Immunology & Genetics, Faculty of Health Sciences, Ben-Gurion University of the Negev, Beer Sheva, Israel; [c]National Institute of Advanced Studies, IISc. Campus, Bangalore, India; [d]Mahatma Gandhi Medical Preclinical Research Centre (MGMPRC), Sri Balaji Vidyapeeth (Deemed to-be University), Pillayarkuppam, Puducherry, India

ABSTRACT

Natural products serve as a valuable resource in drug discovery and the identification of bioactive molecules in the field of epimedicine, which targets epigenetic regulator enzymes through epidrugs. In this study, β-1,3-glucan (BG), a natural storage polysaccharide in *Euglena gracilis*, a well-known immunostimulatory agent, is propounded as a promising epidrug. To elucidate the therapeutic efficacy of BG against ovarian cancer, the molecular interactions between BG and epigenetic regulators, Protein Arginine Methyltransferases (PRMTs) and Sirtuins (SIRTs) were investigated using computational methods followed by *in vitro* gene expression studies in SKOV-3 ovarian cancer cell line. The binding energies of PRMT5 and SIRT5 against BG were observed as −65.5 and −68.2 kcal/mol, respectively. The *in vitro* cytotoxic effects of BG against human ovarian cancer cell line, SKOV-3 showed an IC_{50} of 150 μg/mL at 48 h. Significant epigenetic modifications were observed to be influenced by BG which increased the gene expression of PRMT5, SIRT5 and Nrf1/2 to 0.3, 0.5, and 0.7 fold-change respectively while the Nrf1/2 plasmid showed reduced reporter activity by 29%. Collectively, both *in silico* and *in vitro* studies provided valuable insights into the epigenetic regulation of PRMT5 and SIRT5 by BG *via* Nrf1/2. Nonetheless, further preclinical and clinical investigations are essential to validate the therapeutic properties of BG as an epidrug against ovarian cancer.

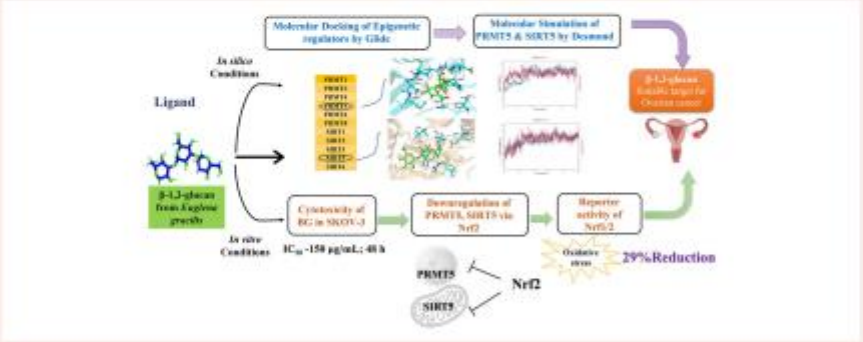

ARTICLE HISTORY
Received 20 September 2023
Accepted 23 April 2024

KEYWORDS
Natural products; epigenetics; β-1; 3-glucan; PRMT; SIRT; ovarian cancer

1. Introduction

Ovarian cancer, the prevailing gynaecological malignancy, is associated with unfavourable prognosis and challenges in biomarker identification. Despite the availability of treatment strategies and drugs, the survival rate of patients with ovarian cancer remains low. Hence, there is an urgent need to explore alternative therapeutic options to overcome drug resistance and toxicity (Akter et al., 2022). A promising approach involves combining epigenetic therapy with DNA chromatin modification to address these limitations while minimizing adverse side effects (Moufarrij et al., 2019). Epigenetic regulators play a critical role in regulating gene expression without modifying DNA sequences, and are also involved in ovarian cancer tumorigenesis (Cheng et al., 2019). Among several epigenetic markers, Protein Arginine methyltransferases (PRMTs) and Sirtuins (SIRTs), belonging to

CONTACT Veni Subramanyam venis@mgmari.sbvu.ac.in; Kumar Chinnadurai rajkumarc@mgmari.sbvu.ac.in
*Equal first author contribution.
Supplemental data for this article can be accessed online at https://doi.org/10.1080/07391102.2024.2425832.
© 2024 Informa UK Limited, trading as Taylor & Francis Group

ScienceDirect

Cancer Stem Cells and Signaling Pathways
2024, Pages 227-242

Chapter 12 - Epigenetic modification: key regulator of reprogramming in cancer stem cells

Varsha Virendra Palol [1], Suresh Kumar Saravanan [2], Raj Kumar Chinnadurai [1], Veni Subramanyam [1]

[1] Mahatma Gandhi Medical Advanced Research Institute (MGMARI), Sri Balaji Vidyapeeth (Deemed to-be University), Puducherry, India
[2] Mahatma Gandhi Medical Preclinical Research Centre (MGMPRC), Sri Balaji Vidyapeeth (Deemed to-be University), Puducherry, India

Available online 3 November 2023, Version of Record 3 November 2023.

What do these dates mean?

Show less

Outline | Share Cite

https://doi.org/10.1016/B978-0-443-13212-4.00017-9

Get rights and content

Abstract

Cancer stem cells (CSCs) are tumor subsets that can self-renew, differentiate into various tumor lineages, and induce dynamic cellular phenotypic changes from epithelial to mesenchymal transition responsible for drug resistance and cancer relapse. Metastasis and malignancy are regulated by network of molecular mechanism. Heterogeneity of CSCs depends on plasticity of CSCs controlled by DNA mutations, epigenetic changes, and genomic rearrangements in several signaling pathways. The machinery of epigenetics potentiates reprogramming of heterogeneous tumor phenotype into homogeneous normal cells by DNA methylation, histone deacetylation, and noncoding RNAs, which are of therapeutic interest to target CSCs. The treatment strategies started aiming to control the link of formation, maintenance, activation, and transformation of CSCs using epigenetic drugs. The advancement of treatment with targeted mechanisms includes several epigenetic inhibitors in clinical trials. This book chapter focuses on the underlying epigenetic reprogramming mechanisms in CSCs with respect to treatment strategies and therapies employed in research and progressed into clinical trials.

Recommended articles

PODIUM/ POSTER PRESENTATIONS AT INTERNATIONAL CONFERENCE

MIT School of
Bioengineering Sciences & Research
Breathe Life into Engineering Career!

MIT-ADT UNIVERSITY
PUNE, INDIA
A Leap Towards The World Class Education

5th INTERNATIONAL CONFERENCE ON RECENT TRENDS IN BIOENGINEERING
(ICRTB 2022)
February 12-13, 2022

CERTIFICATE

This is to certify that Dr/Mr/Ms VARSHA V
from CENTRAL INTER-DISCIPLINARY RESEARCH FACILITY, SRI BALAJI VIDYAPEETH
presented a poster/paper entitled ANTI-CANCER EFFECT OF NOVEL NANO-FORMULATIONS OF BETAGLUCANS DERIVED FROM EUGLENA GRACILIS AND THE ROLE OF EPIGENETIC FACTORS IN OVARIAN CANCER: AN IN VITRO STUDY
in the conference organised by MIT School of Bioengineering Sciences & Research at MIT-ADT University, Pune, India from February 12- 13, 2022. He/She has won FIRST prize at the conference. The organizing committee thanks you for your efforts and participation.

Dr. Renu Vyas	Prof. Vinayak Ghaisas	Prof. Dr. Mangesh T. Karad	Hon.Prof. Dr. Vishwanath D. Karad
Convenor Organizing Committee, ICRTB 2022 Head of School, MIT School of Bioengineering Sciences & Research	Director, MIT School of Bioengineering Sciences & Research Trustee, MIT Group of Institutions	Trustee, MIT Group of Institutions Executive President and Vice Chancellor, MIT ADT University	Founder President, MIT Group of Institutions President, MIT ADT University

PONDICHERRY UNIVERSITY
पांडिचेरी विश्वविद्यालय புதுவைப் பல்கலைக்கழகம்

DDTR-2021

CERTIFICATE OF MERIT

THIS CERTIFICATE IS AWARDED TO

VARSHA V, Central Inter-Disciplinary Research Facility, Sri Balaji Vidyapeeth FOR ACHIEVING THE *FIRST* PLACE

IN THE E-POSTER PRESENTATION COMPETITION

HELD DURING THE

INTERNATIONAL VIRTUAL CONFERENCE ON DRUG DISCOVERY AND TRANSLATIONAL RESEARCH

HOSTED BY

DEPARTMENT OF BIOCHEMISTARY & MOLECULAR BIOLOGY, PONDICHERRY UNIVERSITY

DURING FEBRUARY 25-26, 2021.

Dr. R. Rukkumani	Dr. S. Sudha Rani	Dr. C. Subbulakshmi
CO-ORDINATOR	CO-ORGANIZER	ORGANIZER